

Compatibility and simulation of the heating up of the propellant charge body of a high precision machine gun

Manfred A. Bohn *, Axel Pfersmann **

*) Fraunhofer ICT, D-76318 Pfinztal, Germany

***) Diehl BGT Defence GmbH & Co. KG, D-90552 Roethenbach a. d. Pegnitz, Germany

Abstract

The new precision machine gun in development at company Diehl uses a propellant charge without any case. It is based on consolidated NC double base ball powder. For ballistic reasons a defined distance between propellant charge body (PB) and the wall of the combustion chamber must be adjusted and for this a new feature was developed in cooperation with Fraunhofer ICT. The distance is achieved with foam stripes based on polyurethane energized by HMX. To avoid a degradation of the ballistic properties during use time, compatibility investigations using heat flow microcalorimetry have been performed to select suitable foam formulations. For this special assessment the criteria have been developed. A further design feature is a thermal insulation between the combustion chamber wall and the PB. This is also achieved by the energetic PUR foam. To design and predict this thermal insulation, FE calculations have been made using the thermal property and decomposition characteristics of the energetic foam and the PB, which have been parameterized by iso-conversional analysis. The calculations have been compared with real measurements of the times to autoignition at different burning chamber temperatures.

Keywords

Caseless propellant charge, NC-based propellant, energetic PUR foam, compatibility, microcalorimetry, iso-conversional analysis, FE calculations, times to autoignition.

1. Introduction

The new demands with respect to costs and efficiency in tactical response have been one motivation for company Diehl to develop a new weapon system, which allows fast and very precise counteracting especially in improvised and high mobility attack situations. The state of design is a machine gun for 12.7 mm caliber with a special design in loading projectile and propellant charge /1/. Both are separated and loaded separately in two rotating dual chamber devices. The projectile chamber is also separated from the barrel. A further feature is the propellant charge, without casing and made from consolidated double base ball powder. This new loading system ensures precise positioning of the projectile and avoiding 'lateral' effects as they occur with conventional ammunition.

The operation principle of the machine gun is shown in the Figures 1 to 4. Fig. 5 presents a view of aligned projectile and propellant charge body in firing position. In Fig. 6 photographs of the propellant body can be seen together with a schematic scetch of it. On the

Paper 27, pages 27-1 to 27-35 in Proceedings of the 43rd International Annual Conference of ICT on 'Energetic Materials – Synthesis, Characterisation, Processing', June 26 to 29, 2012, Karlsruhe, Germany. ISSN 0722-4087. Fraunhofer-Institut fuer Chemische Technologie (ICT), D-76318 Pfinztal. Germany.

© Fraunhofer ICT, Pfinztal, Germany.

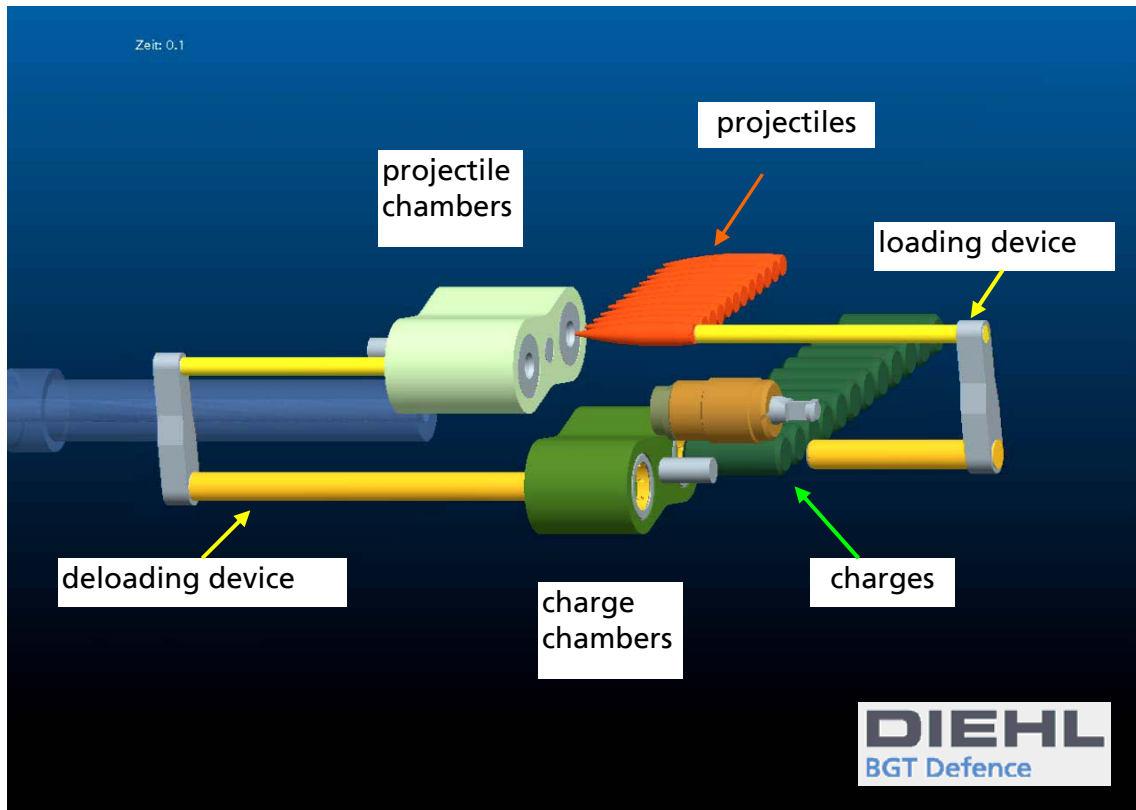


Fig. 1: Situation before starting cycles: loading and firing. Above double the projectile chamber, below the double charge chamber.

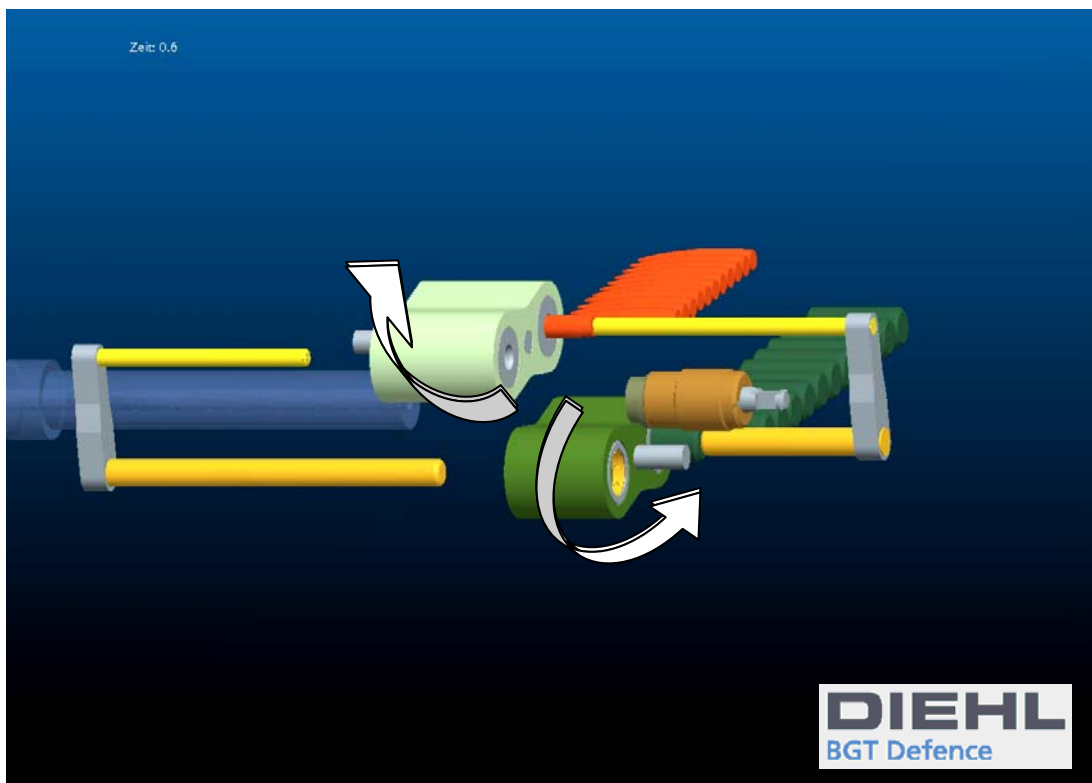


Fig. 2: Loading the projectile (above) and the charge (below) simultaneously in the two different chambers. After the loading, the two double chambers counter rotate by 90° into the firing position, where loaded projectile chamber and loaded charge chamber are in line.

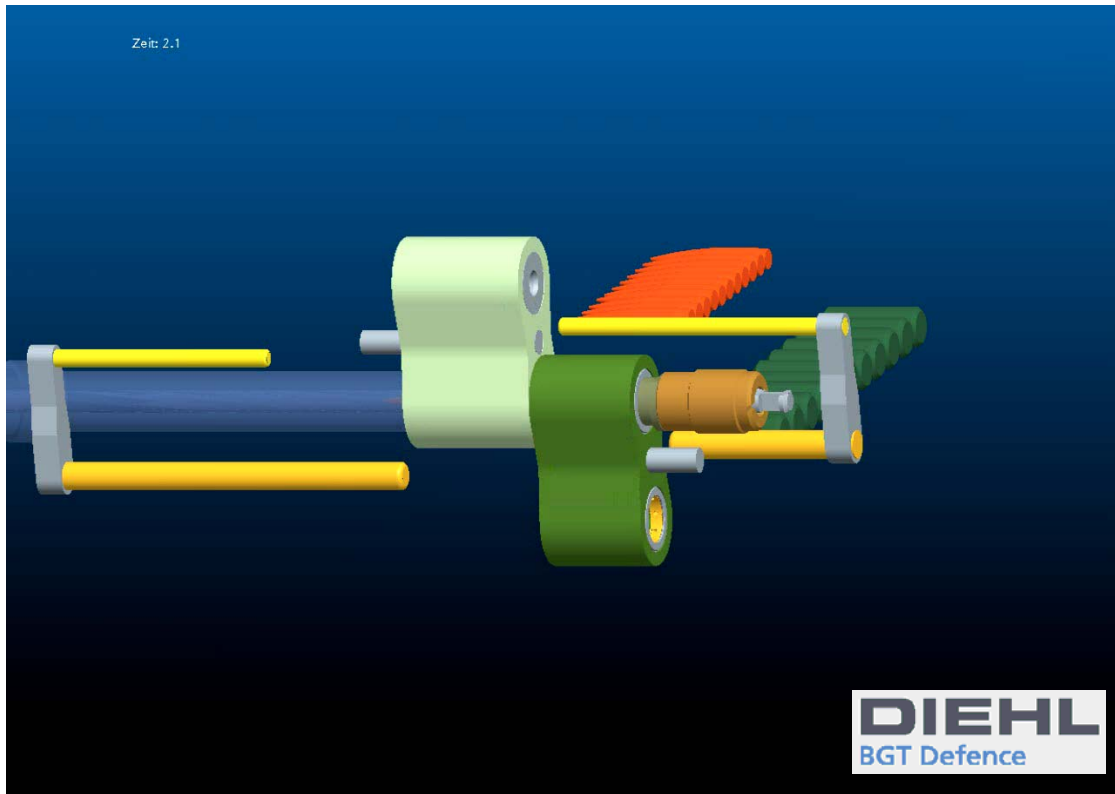


Fig. 3: Firing position, the breech of the charge chamber is closed. After firing the two double chambers rotate further by 90° to the loading position.

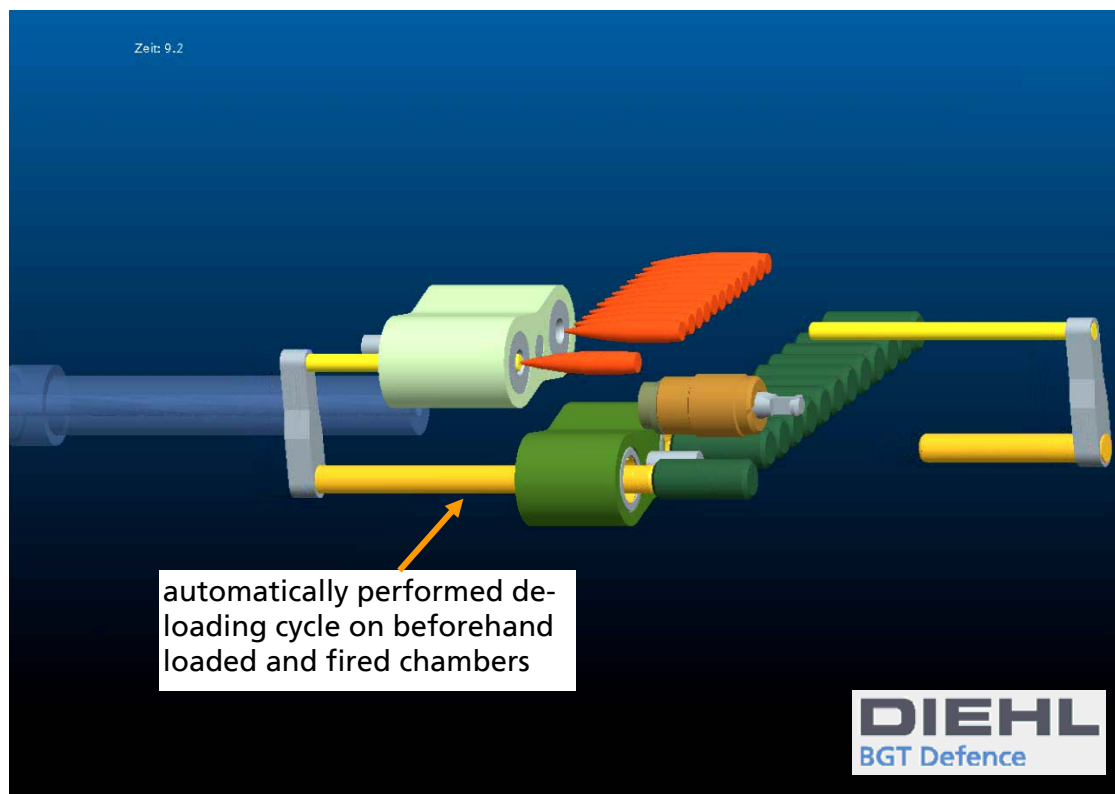


Fig. 4: Before loading again, the two chambers from the beforehand firing position are checked by the de-loading device. If the shot would have been unsuccessful, these chambers would be cleared before their next loading.

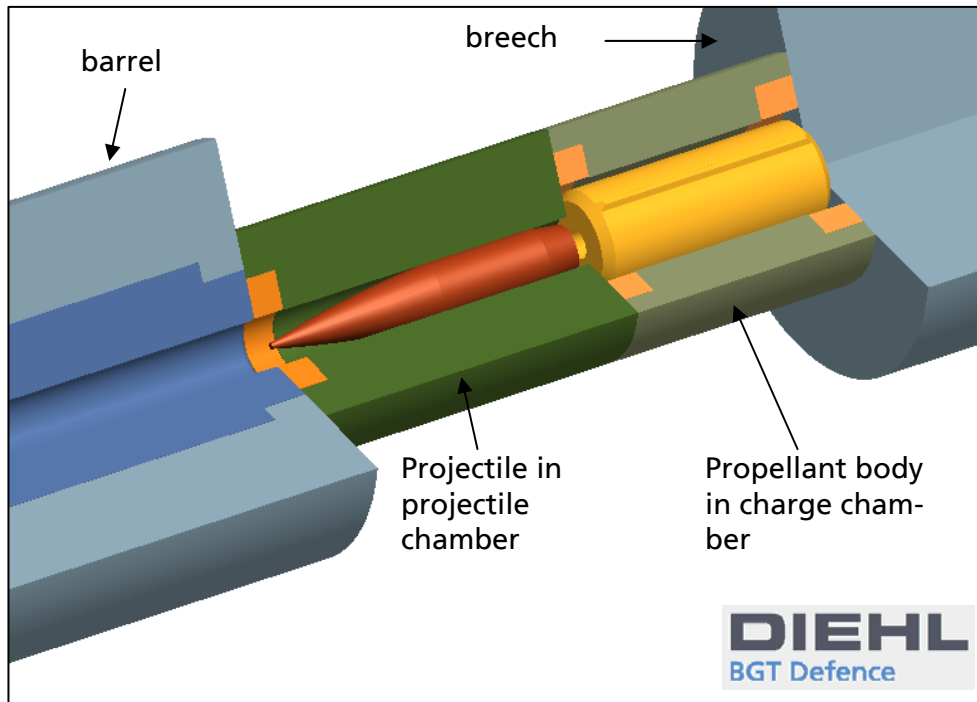


Fig. 5: Expanded view of projectile and charge aligned in firing position.

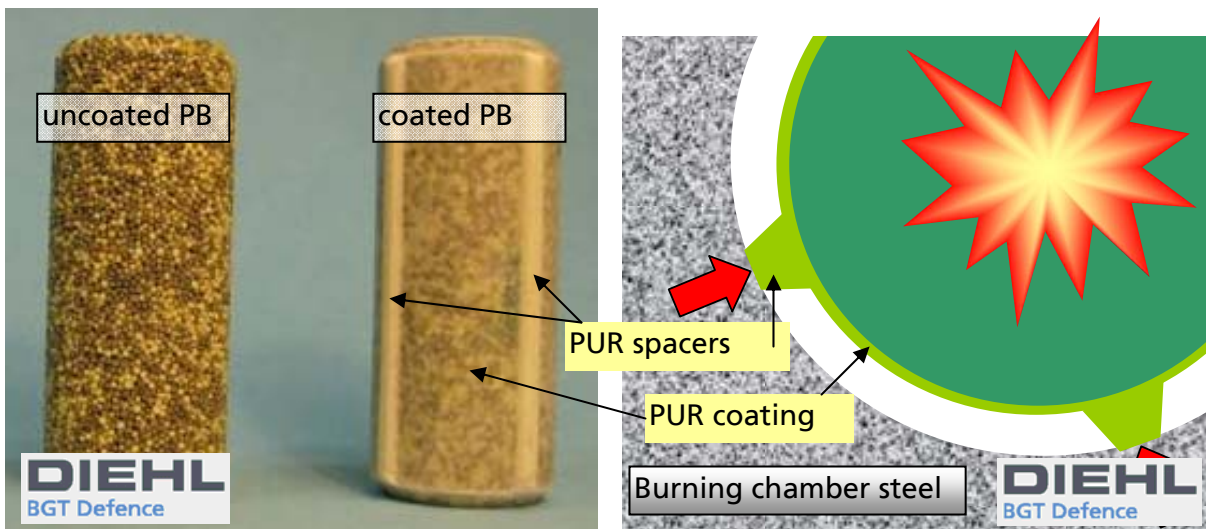


Fig. 6: Left: Photographs of the propellant body PB, made from glued ball powder, in uncoated form and coated with energetic PUR foam and equipped with four spacers, also made from energetic PUR foam. Right a schematic scetch of the PB in the burning chamber.

left side of Fig. 6, the left part shows the uncoated body made from ball powder, the right part shows the PUR coated body and the applied PUR spacers. Besides the precision loading advantage the thermal load on the projectile and charge chambers is reduced in using the double chamber system for both ammunition parts. This increases again the precision and helps to avoid cook-off effects of the NC-based charge body. This charge is made from conventional double base ball powder consolidated by glueing the balls together. The glueing is made in such a way that during ignition the body desintegrates easily into the balls and the known and precisely adjustable ballistics of phlegmatized ball powder can be used in propelling the projectile. To facilitate the fragmentation the propellant charge body (PB) should have a free space to the combustion

chamber wall. This is achieved by spacer stripes and a central bore in the body. In order to have complete combustion of stripes they are made from HMX (octogen) filled polyurethane foam. Additionally to the spacers a coating is applied on the propellant body made with the same energetic PUR foam. The demands on the coating and spacer material are: (i) the coating must form a closed surface; (ii) it must have the necessary strength; (iii) it must be combustible; (iv) it must have a high autoignition temperature; (v) it should have a low heat conductivity; (vi) last but not least it must be compatible with the propellant body material. The PUR foam material for the spacers and the coating was developed by Fraunhofer ICT applying the experience gained with the work on caseless foamed propellant charges for telescoping projectiles /2, 3/. During the time period from loaded to unloaded position no cook-off may be caused by the heated up combustion chamber walls.

The two demands compatibility and cook-off probability have been investigated by Fraunhofer ICT. The compatibility was determined using heat flow microcalorimetry /4/. The cook-off behaviour of the spacers and the PB was evaluated by FE (finite element) calculations using the thermal properties and decomposition behaviour of the PUR foam material and the PB. The cook-off behaviour was also experimentally determined by company Diehl, after the simulations have been performed.

2. Compatibility investigations between PUR foam and PB

2.1 Prerequisites for the compatibility assessment

For assessing compatibility or reactivity the best is to use a procedure based on the excess chemical conversion /4/. The excess reaction part or the excess conversion is obtained **by the difference** of measured quantities P. This means the values of the single components are subtracted from the value of the mixture. This is analogous to the thermodynamic description of mixtures with excess quantities. The here used reactivity functions $R_p(t,T)$ are defined as the difference of measured quantities P, Eq.(1), which are scaled in substance amount and taken as absolute, Eq.(1), or reference value normalized quantities, Eq.(2). They can be formed also with mixture ratios based on molar amount, volume, surface or number of reactive groups. With 1:1 mixtures by mass one has $M_{G1}/M_G = 0.5$ in the equations below. Eq.(2) shows the fully normalized reactivity expression $R_{Pr}(t,T)$, which is a conversion quantity and correctly $R_{Pr}(t,T)$ is named excess conversion function or excess reaction conversion function or inter-component reaction conversion function. Note: R_p and R_{Pr} ranges from negative to positive values.

$$(1) \quad R_p(t,T) = \frac{P_G(t,T)}{M_G} - \frac{M_{G,1}}{M_G} \cdot \left(\frac{P_1(t,T)}{M_1} \right) - \frac{M_{G,2}}{M_G} \cdot \left(\frac{P_2(t,T)}{M_2} \right) \quad \text{excess reaction function}$$

$$(2) \quad R_{Pr}(t,T) = \frac{\frac{P_G(t,T)}{M_G}}{P_{G,ref}} - \frac{M_{G,1}}{M_G} \cdot \left(\frac{\frac{P_1(t,T)}{M_1}}{P_{1,ref}} \right) - \frac{M_{G,2}}{M_G} \cdot \left(\frac{\frac{P_2(t,T)}{M_2}}{P_{2,ref}} \right) \quad \begin{array}{l} \text{excess reaction conversion} \\ \text{function or} \\ \text{inter-component reaction} \\ \text{conversion function} \end{array}$$

Meaning of symbols in Eq.(1) and Eq.(2):

R_p reactivity function or excess reaction function, determined with measurement quantity P

R_{Pr} normalized reactivity function or excess reaction conversion function, determined with measurement quantity P and the corresponding reference values P_{ref}

- M_G mass of the mixture at $t=0$
 M_{G1} mass of component 1 in mixture at $t=0$
 M_{G2} mass of component 2 in mixture at $t=0$
 P_G measurement quantity P of mixture
 P_1 measurement quantity P of component 1, with sample mass M_1 at $t=0$
 P_2 measurement quantity P of component 2, with sample mass M_2 at $t=0$
 $P_{G,ref}$ reference value of measurement quantity P of mixture, amount normalized
 $P_{1,ref}$ reference value of measurement quantity P of component 1, amount normalized
 $P_{2,ref}$ reference value of measurement quantity P of component 2, amount normalized

With heat generation Q , mostly one uses the excess reaction function, Eq.(3) /4, 5/. In this equation $Q_i(t,T)$ are already initial mass normalized. With the normalization by the end values $Q_i(t_e)$ or also the reference values Q_{ref} later used, the excess conversion function is obtained, Eq.(4). To find the appropriate values for the normalization constants $Q_i(t_e)$ is not straightforward. The heat of explosions Q_{EX} are taken often, but from the view of reaction kinetics they are not the correct data. The quantities $Q_i(t_e,T)$ are the reference quantities, which do no longer change in value beyond the time t_e . The time t_e is an end time at the measurement temperature T . With heat generation one has to measure up to such an end time $t_e(T)$ to get the corresponding normalization factor, which is from reaction kinetic view the correct one. However to get these data with real microcalorimetric measurements in the temperature range 60°C to 100°C is mostly not affordable because of the long to very long measurement times, up to months and even years range. Therefore the thermodynamically determined Q_{EX} values are taken here.

$$(3) \quad R_Q(t, T) = Q_G(t, T) - \frac{M_{G,1}(0)}{M_G(0)} \cdot Q_1(t, T) - \frac{M_{G,2}(0)}{M_G(0)} \cdot Q_2(t, T)$$

$$(4) \quad R_{Qr}(t, T) = \frac{Q_G(t, T)}{Q_G(t_e, T)} - \frac{M_{G,1}(0)}{M_G(0)} \cdot \left(\frac{Q_1(t, T)}{Q_1(t_e, T)} \right) - \frac{M_{G,2}(0)}{M_G(0)} \cdot \left(\frac{Q_2(t, T)}{Q_2(t_e, T)} \right)$$

In Table 1 time-temperature loads are given, which all exert the same thermal load and representing the load at 25°C over 10 years /6, 7/. To have a sufficient in-service time prediction for the evaluation made here the load of 15 days at 80°C is chosen, which represents 15 years at 25°C .

The next important point is to determine the limit values for R_Q at different total reference values of Q_{ref} for the mixtures investigated. The reference values range between about 2500 and 3500 J/g. An additional conversion of 1% is allowed at the thermal load of 80°C over 15 days. This is somewhat more restrictive than given in STANAG 4147 /5/, which allows about 1% (30 J/g) at the thermal load of 80°C over 10 days. The resulting R_Q values for the three Q_{ref} values are given in Table 2, also at additional conversions smaller than 1%. The limit values R_Q are thereafter ± 25 , ± 30 and ± 35 J/g at Q_{ref} values of 2500, 3000 and 3500 J/g.

If the ratio of the two components is not 1:1 per mass, then a scaling of the limit values has to be applied according to Eq.(5), see /4/. This scaling assumes a linear behaviour with the mixture ratio. Table 3 lists the scaled limit values starting with given ones for 1:1 mixtures.

$$(5) \quad R_P^f = \frac{2 \cdot f \cdot R_P^{1:1}}{f + 1} \quad \text{with } 0 \leq f \leq 1$$

Table 1: Test times t_m and corresponding test temperatures T_m to exert the same thermal equivalent load as it is done by storage at 25°C over 10 years, see /6, 7/. Additionally given are the corresponding limits of the heat generation rate values applicable for determining the stability of NC-based propellants.

T_m [°C]	t_m [d]	$(dQ/dt)_L$ [μ W/g]	T_m [°C]	t_m [d]	$(dQ/dt)_L$ [μ W/g]
60	123	9.8	78	13.4	90.0
62	95.0	12.6	80	10.6	114
64	73.6	16.3	82	8.41	143
65	64.9	18.5	84	6.70	179
66	57.2	21.0	85	5.98	201
68	44.6	27.0	86	5.35	225
70	34.8	34.5	88	4.28	281
71	30.8	39.0	89	3.83	314
72	27.3	44.0	90	3.43	350
74	21.5	56.0	95	2.00	600
75	19.0	63.1	100	1.184	1015
76	16.9	71.1	105	0.710	1693

Table 2: Allowed additional reactivity R_Q and linearly scaled additional reactivity rate dR_Q/dt at preset allowed additional conversions using three reference values Q_{ref} and several thermal loads.

thermal load		allowed additional conversion [%]	$Q_{ref} = 2500\text{J/g}$		$Q_{ref} = 3000\text{J/g}$		$Q_{ref} = 3500\text{J/g}$	
T [°C]	t [d]		$\pm R_Q$ [J/g]	$\pm dR_Q/dt$ [μ W/g]	$\pm R_Q$ [J/g]	$\pm dR_Q/dt$ [μ W/g]	$\pm R_Q$ [J/g]	$\pm dR_Q/dt$ [μ W/g]
80	15	0.50	12.5	9.7	15	11.6	17.5	13.5
80	15	0.60	15	11.6	18	13.9	21	16.2
80	15	0.70	17.5	13.5	21	16.2	24.5	18.9
80	15	1.00	25	19.3	30	23.2	35	27.0

Table 3: Change of limit values R_Q when mixture ratio is not 1: 1

$\pm R_Q $ [J/g] for mixture 1 : 1	25	25	30	30	35	35
mixture ratio f (as 1 : f)	0.25	0.5	0.25	0.5	0.25	0.5
resulting $\pm R_Q $ [J/g] for mixture 1 : f	10	16.7	12	20	14	23.3

2.2 Compatibility between glue and the two propellants PB and A5023

Table 4 compiles the data of the two propellants and their mixtures with the glue. Because of the ratio 4:1 per mass between propellant and glue the applicable limit values have been scaled down from 25 J/g to 10 J/g according to Eq.(5). In Fig. 7 the stability of the three substances can be seen. Shown are two parallel measurements for each one. The ball powder has the highest heat generation rate (HGR) but it is still significantly be-

low the allowed limit of $114 \mu\text{W/g}$ at 80°C over 10.6 days /6, 7/. Fig. 8 presents the HGR and HG (heat generation Q) of the two mixtures. With the data presented in Fig. 7 and 8 the reactivity functions are calculated according to Eq.(3). The reactivity rate function dR_Q/dt is calculated analogously using the heat generation rate data dQ/dt instead of the Q data. In the Fig. 9 and the Fig. 10 the reactivity rate function dR_Q/dt and the reactivity function R_Q of the double base ball powder with glue and the single base propellant A5023 with glue can be seen. The reactivity functions R_Q stay below the limit value of 10 J/g during the measurement time of 15 days at 80°C , so the glue is compatible with both propellants.

Table 4: Basic data of the single components double base BP, single base GP A5023 (20mm machine gun) and the glue as well as of the mixtures propellant - glue.

single component or mixture	Q _{ex} (water liquid) [J/g]	Q _{ex} (water gaseous) [J/g]	generated gas volume (at 25°C) [ml/g]	specific energy (force) [J/g]	Applicable limit $\pm R_Q $ [J/g]
ball powder (BP)	3662	3383	833	992	-
A5023 as reference	3375	3129	868	941	-
glue	1454	980	556	263	-
BP - glue 4:1 per mass	2519	2294	943	667	from 25 to 10
A5023 - glue 4:1 per mass	2436	2212	938	648	from 25 to 10

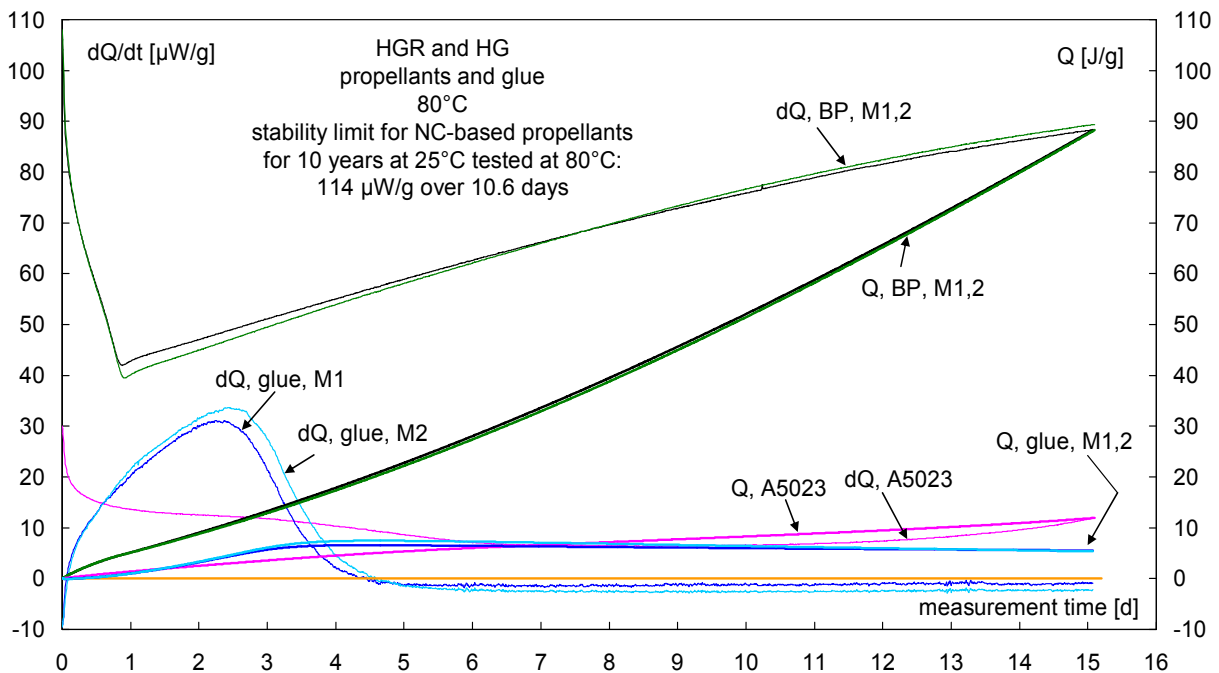


Fig. 7: HGR and HG of the components involved in the compatibility investigation. The ball powder fulfils the demand of STANAG 4582. Its HGR stays below $114 \mu\text{W/g}$ even up to 15 days. The reference propellant A5023 is very stable, because it is a single base propellant and uses not KNO_3 as flash reducer.

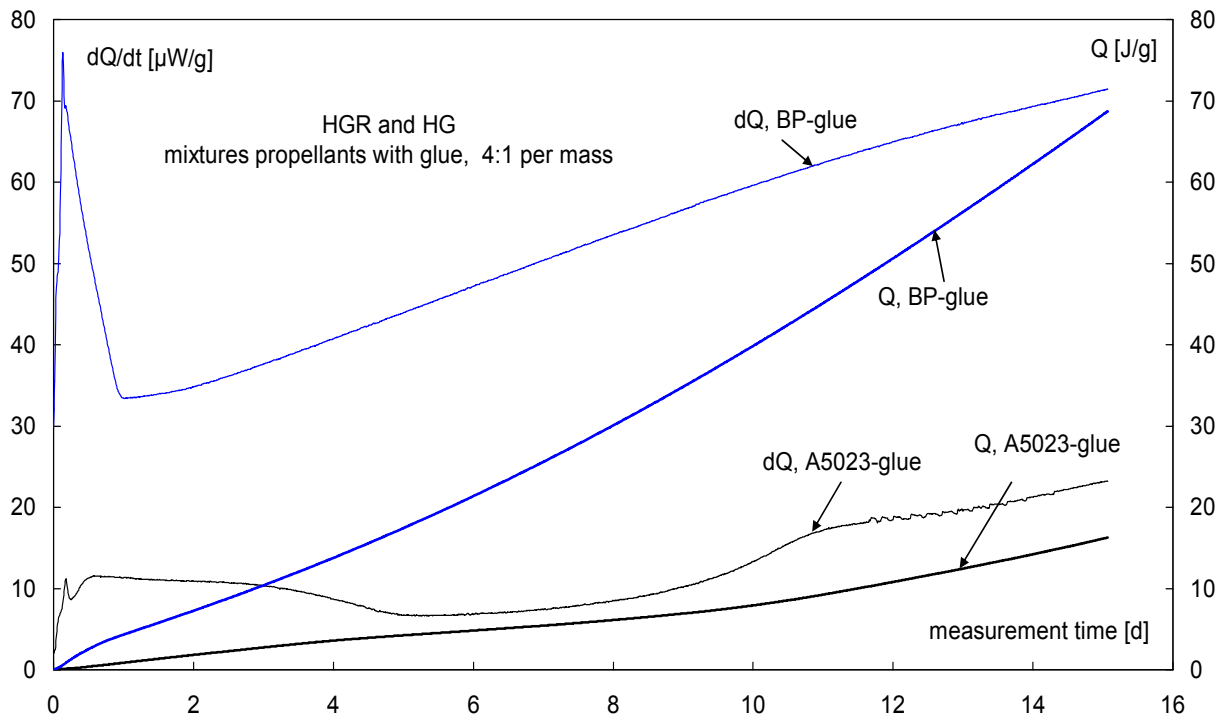


Fig. 8: HGR and HG of the mixtures propellant with glue. A ratio of 4:1 is used here.

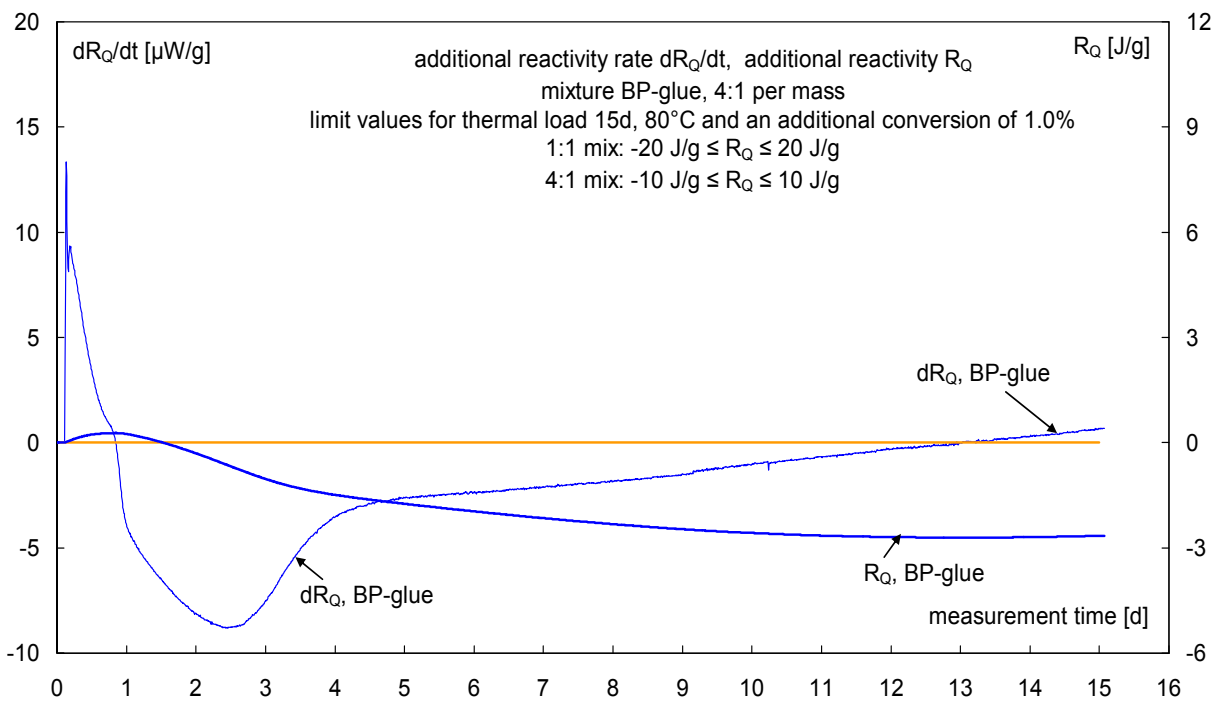


Fig. 9: Reactivity rate function dR_Q/dt and reactivity function R_Q of the 4:1 mixture by mass between ball powder BP and glue.

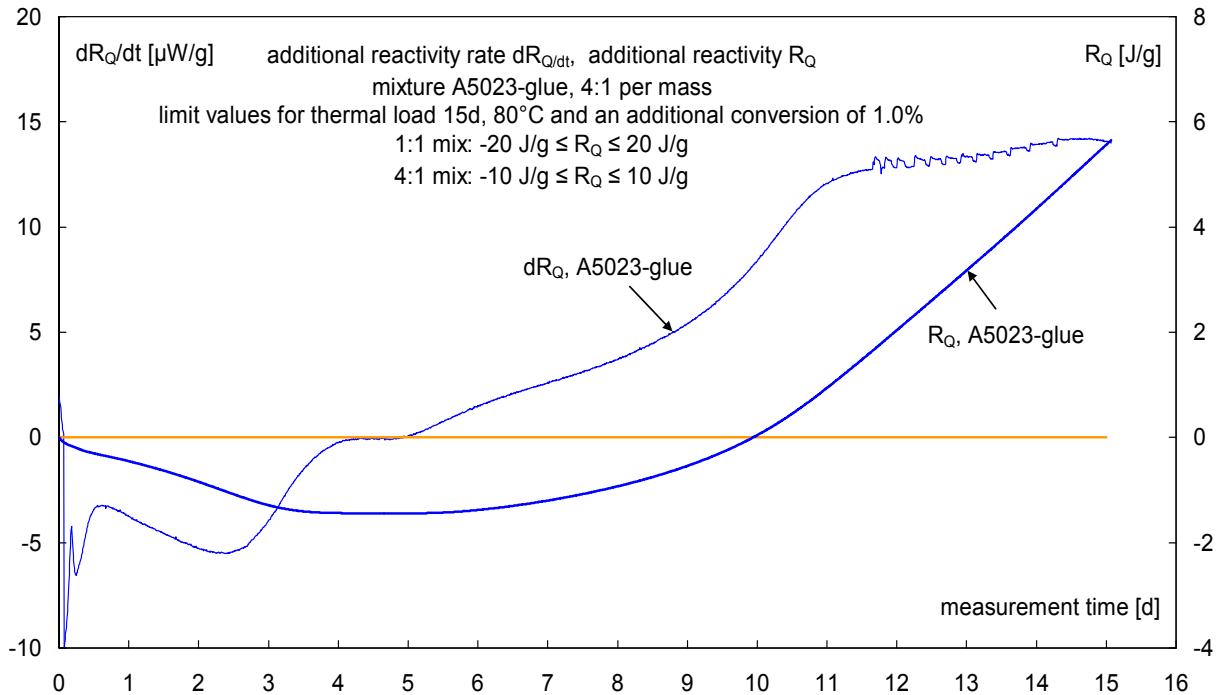


Fig. 10: Reactivity rate function dR_Q/dt and reactivity function R_Q of the 4:1 mixture by mass between propellant A5023 and glue.

2.3 Compatibility between PUR foams and the two propellants PB and A5023 and between PUR foams and the glue

As already shown in session 2.2, in using the reactivity function R_Q for assessing the compatibility, one has to determine individually for each substance pair the corresponding limit value range for R_Q . These data are compiled in Table 5. Again there is a deviation from the 1:1 mixture and the R_Q values have to be adjusted according to Eq.(5). These data are also given in Table 5. In doing so the corresponding values used to calculate the adapted compatibility range have been rounded.

Fig. 11 shows HGR and HG of two pre-selected PUR foam formulations PU8 and PU9. After an initial peak the HGR drops to small values. Fig. 12 presents the HGR and HG of the 1:2 mixtures per mass between the PUR foams and A5023 and Fig. 13 the ones with the ball powder BP.

The reactivity rate functions dR_Q/dt and reactivity functions R_Q between PU8 and PU9 with mixtures of the propellants and the glue are given in the Fig. 14 and Fig. 15, respectively. Glue and A5023 are well compatible with PU8 and PU9. According to the R_Q limit value ranges for the mixtures of PU8 and PU9 with BP, only the PUR foam PU8 fulfils the assessment criteria. Finally this formulation based on an inert PUR system as binder and 50 mass-% HMX was chosen for the application in the spacers and the coating of the consolidated propellant body.

Table 5: Basic data of the single components double base BP, reference single base GP A5023 (20mm machine gun) and the two PUR foams as well as of the mixtures propellant - PUR foam.

single component or mixture	Q _{ex} (water liquid) [J/g]	Q _{ex} (water gaseous) [J/g]	Applicable limit ± R _Q [J/g]
ball powder (BP)	3662	3383	-
A5023 as reference	3375	3129	-
PU8	2510	2289	-
PU9	3300	3150	-
glue	1454	980	-
BP – PU8, 2:1 per mass	3275		from 32 to 22
BP – PU9, 2:1 per mass	3541		from 35 to 23.3
A5023 – PU8, 2:1 per mass	3083		from 30 to 20
A5023 – PU9, 2:1 per mass	3350		from 32 to 22
glue – PU8, 1:2 per mass	2158		from 21 to 14
glue – PU9, 1:2 per mass	2685		from 26 to 17

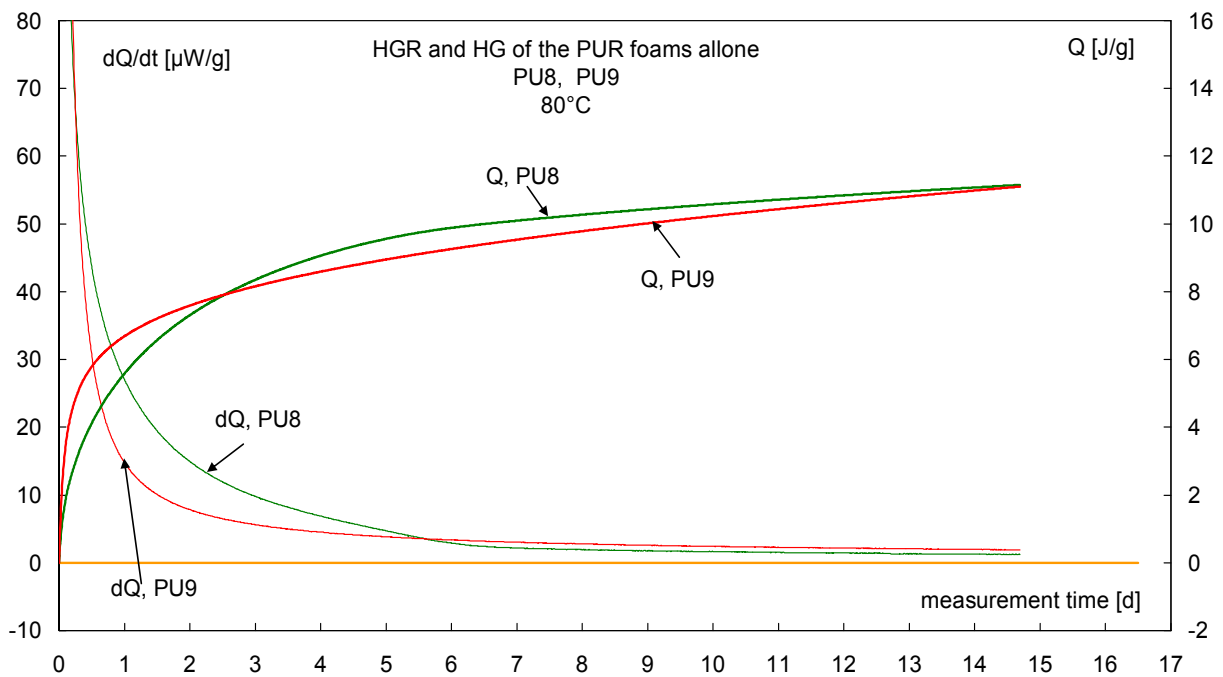


Fig. 11: HGR and HR of the PUR foam formulations PU8 and PU9.

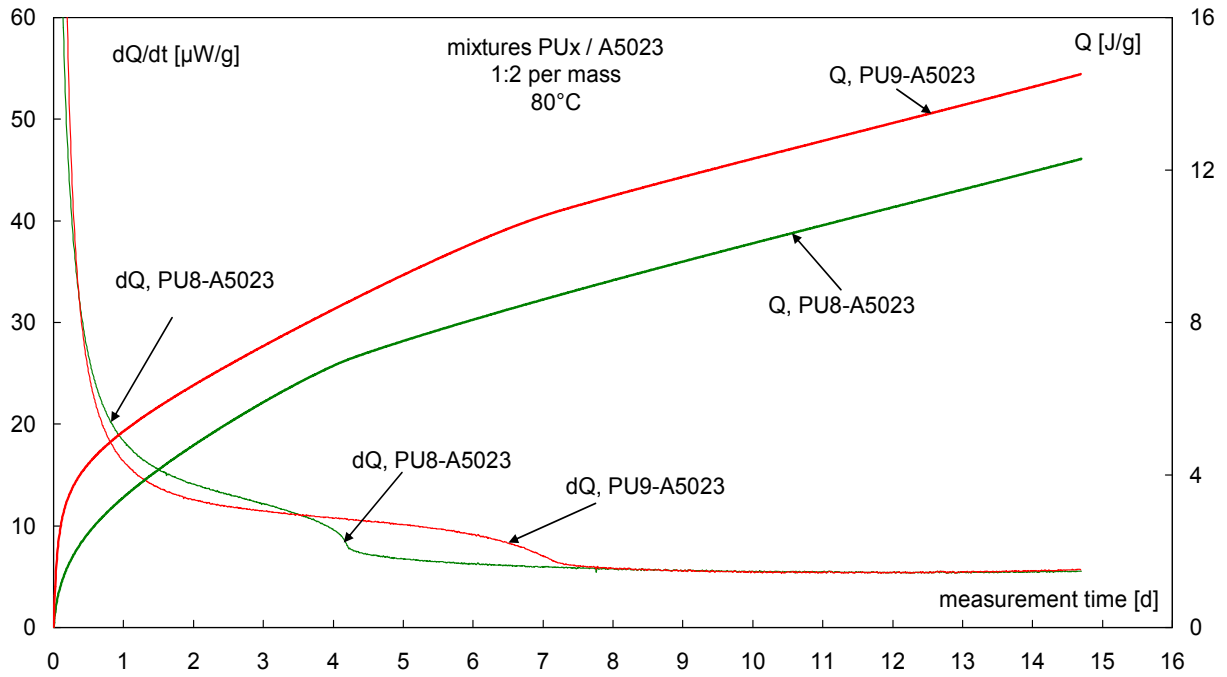


Fig. 12: HGR and HR of the PUR foams PU8 and PU9 in 1:2 mixtures per mass with propellant A5023.

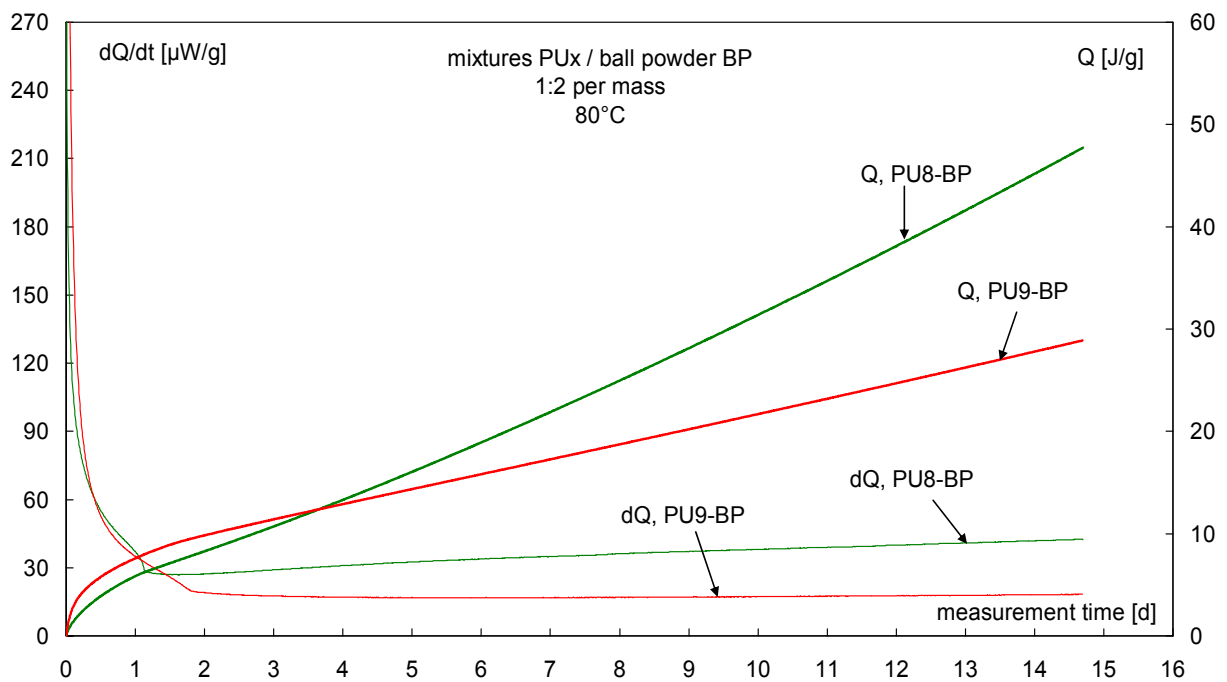


Fig. 13: HGR and HR of the PUR foams PU8 and PU9 in 1:2 mixtures per mass with propellant BP.

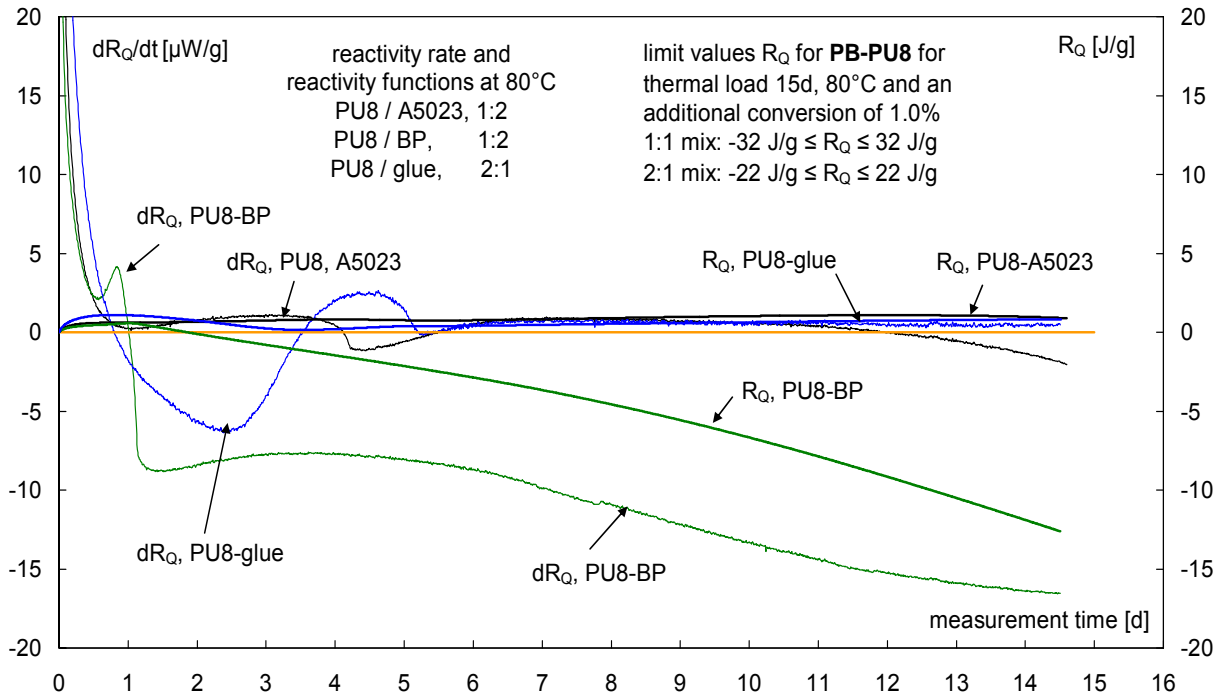


Fig. 14: Reactivity rate function dR_Q/dt and reactivity function R_Q of the 1:2 mixture by mass between PU8 and A5023, PB; R_Q in 2:1 mixture with the glue. The reactivity between ball powder and PU8 is clearly inside the limit range of R_Q of $\pm 22 J/g$ and therewith in the compatibility zone. Glue with $R_Q = \pm 14 J/g$ and propellant A5023 with $R_Q = \pm 20 J/g$ are well compatible with PU8.

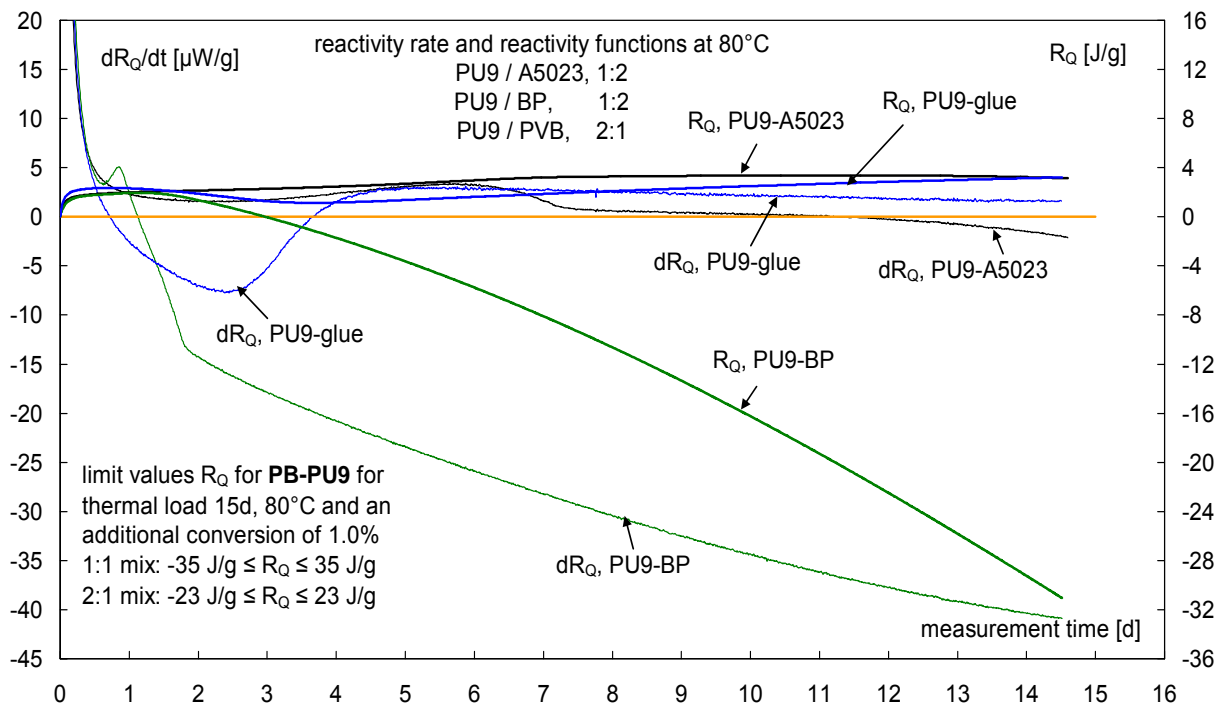


Fig. 15: Reactivity rate function dR_Q/dt and reactivity function R_Q of the 1:2 mixture by mass between PU9 and the propellants A5023, PB; R_Q in 2:1 mixture with glue. The reactivity between ball powder and PU9 is beyond the fixed limit values of $\pm 23.3 J/g$ for R_Q . Glue with $R_Q = \pm 17 J/g$ and propellant A5023 with $R_Q = \pm 22 J/g$ are well compatible with PU9.

3. Simulation of the cook-off behaviour of PUR foam spacer, PUR foam-coating and PB

3.1 Prerequisites needed to perform the simulation

The FE-simulation of the cook-off behaviour is based on the solution of the general heat balance equation including the heat transfer to the reservoir on the outside of the steel body representing the burning chamber. For the simulation calculations the following data are needed:

- Thermal decomposition behaviour, which is determined by DSC in closed pressure resistant crucibles
 - for PUR foam PU8
 - for the propellant body
- Parameterizing of the DSC measurements to be usable in the FE calculations
- Heat conductivity of the PUR foam (formulation PU8)
- Heat conductivity of the propellant body PB
- Specific heat capacity for PUR foam PU8
- Specific heat capacity for propellant body PB
- Mass density for PUR foam PU8
- Mass density for propellant body PB
- Heat conductivity, specific heat capacity, mass density for the steel of the burning chamber and of the air enclosed in the central bore of the PB
- Geometrical dimensions of the arrangement, rotational symmetry is given
- Heat transfer coefficient between outside air, acts here also as heat reservoir, and the steel body

3.2 DSC measurements and Friedman-type data analysis

Fig. 16 shows the DSC measurements on PUR-foam PU8 in closed high pressure crucibles at four heating rates. These data have been subjected to a Friedman-type analysis, means to an iso-conversional analysis, in order to get the activation energy and the pre-exponential factor as function of decomposition conversion, see Fig. 17. In this way one can describe the measurement data in great detail, as long as they are congruent in decomposition behaviour in the temperature range covered by the measurements. This type of analysis is described in /8/, further details can be found in /9, 10, 11/. The AKTS software package was used to perform all the operations and calculations /10/. Fig. 18 presents besides the activation energy also the correlation coefficient of the analysis, which should be mostly in the range 0.95 to 1, which is the case. The Figs 20, 21 and 22 show the same type of data for the ball powder based propellant charge. During the essential parts of PB decomposition conversion the correlation coefficient is near 1. At the beginning and at the end, the correlation coefficient drops because of the generally limited measurement accuracy of the DSC instrument, if one wants to measure the whole decomposition curve in one run. To improve accuracy in these parts several measurements have to be made with adapted sample amounts to improve the quality at least during the first 20% of conversion.

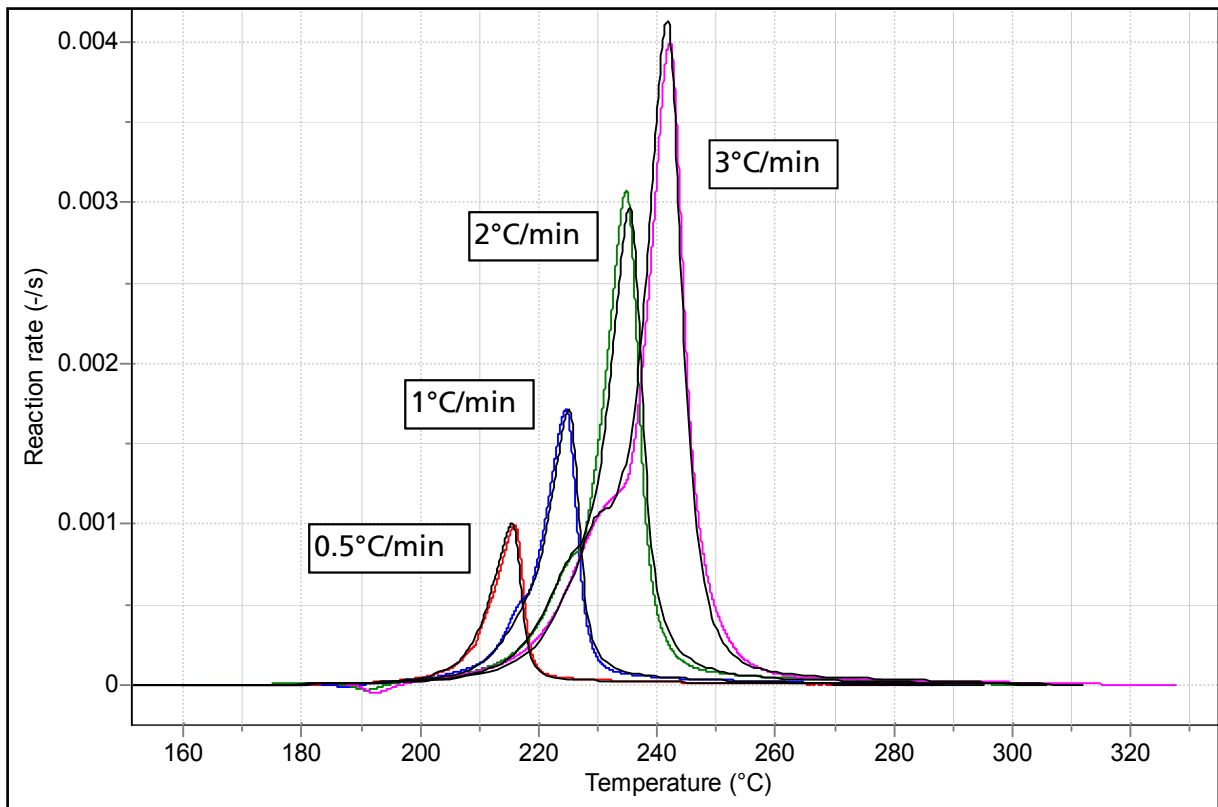


Fig. 16: DSC data of the spacer foam PU8. Measured (coloured) and modelled (black) heat flow curves at the heating rates 0.5, 1, 2, 3 °C/min.

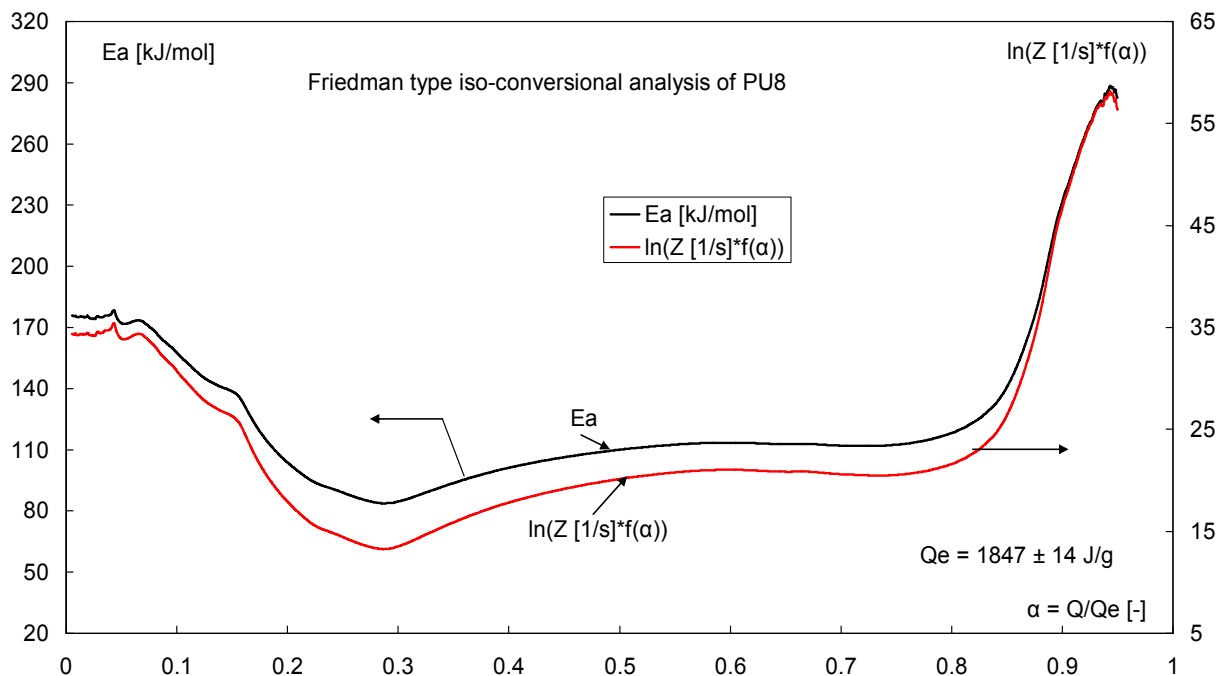


Fig. 17: Result of the Friedman analysis (=differential iso-conversional data analysis) of the DSC data of the spacer foam PU8. Activation energy and pre-exponential factor as function of conversion of the exothermal decomposition reaction.

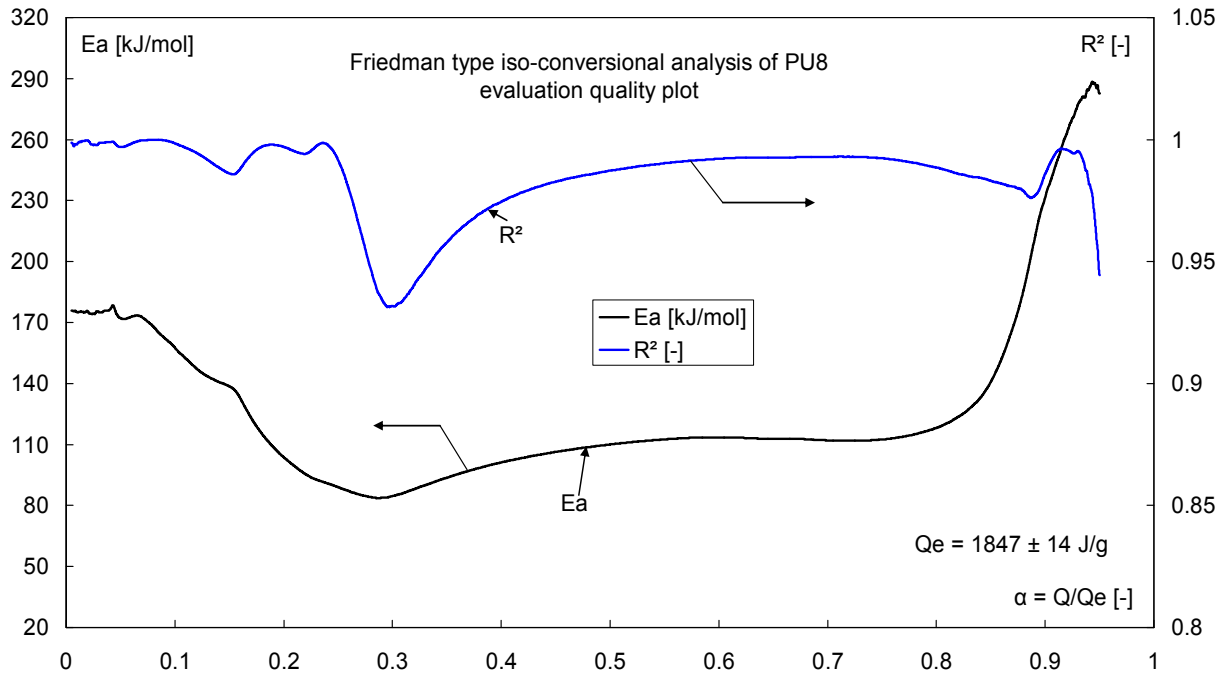


Fig. 18: Evaluation quality plot, showing the correlation coefficient of the Friedman analysis of the DSC data of the spacer foam PU8. Activation energy and correlation coefficient as function of conversion of the exothermal decomposition reaction.

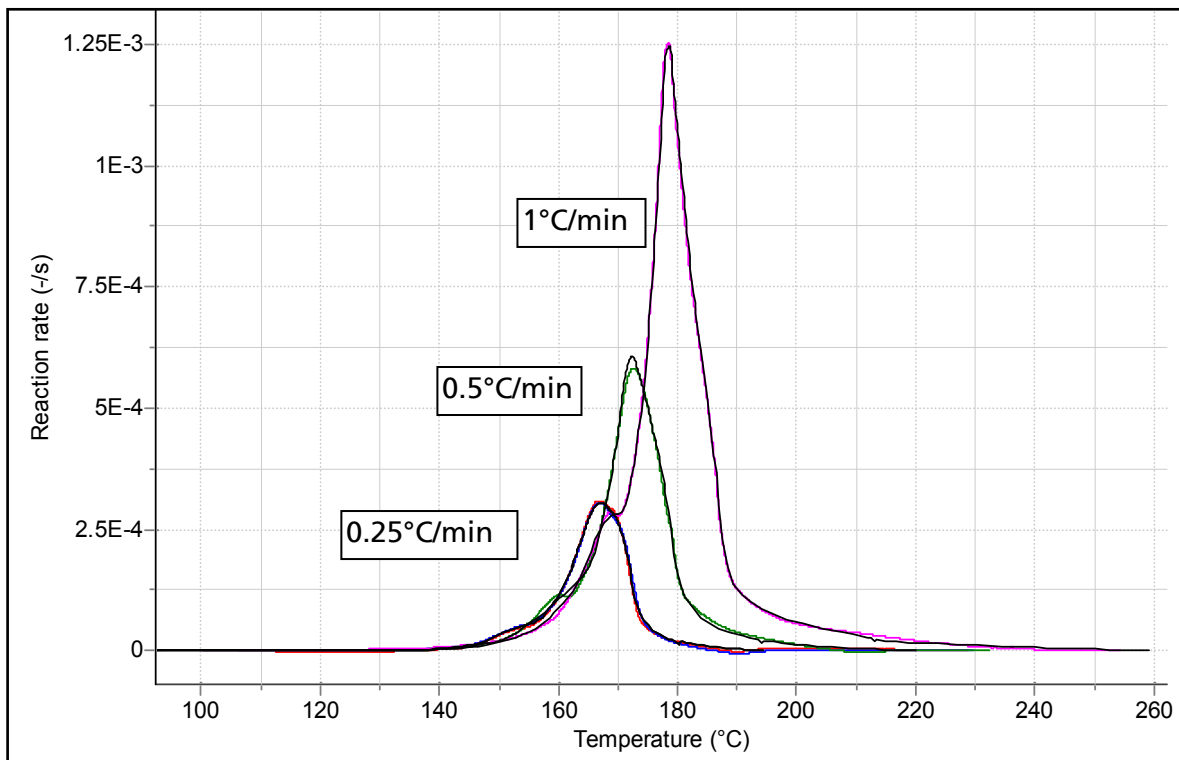


Fig. 19: DSC data of the ball powder based propellant body. Measured (coloured) and modelled (black) heat flow curves at the heating rates 0.25, 0.5, 1 °C/min.

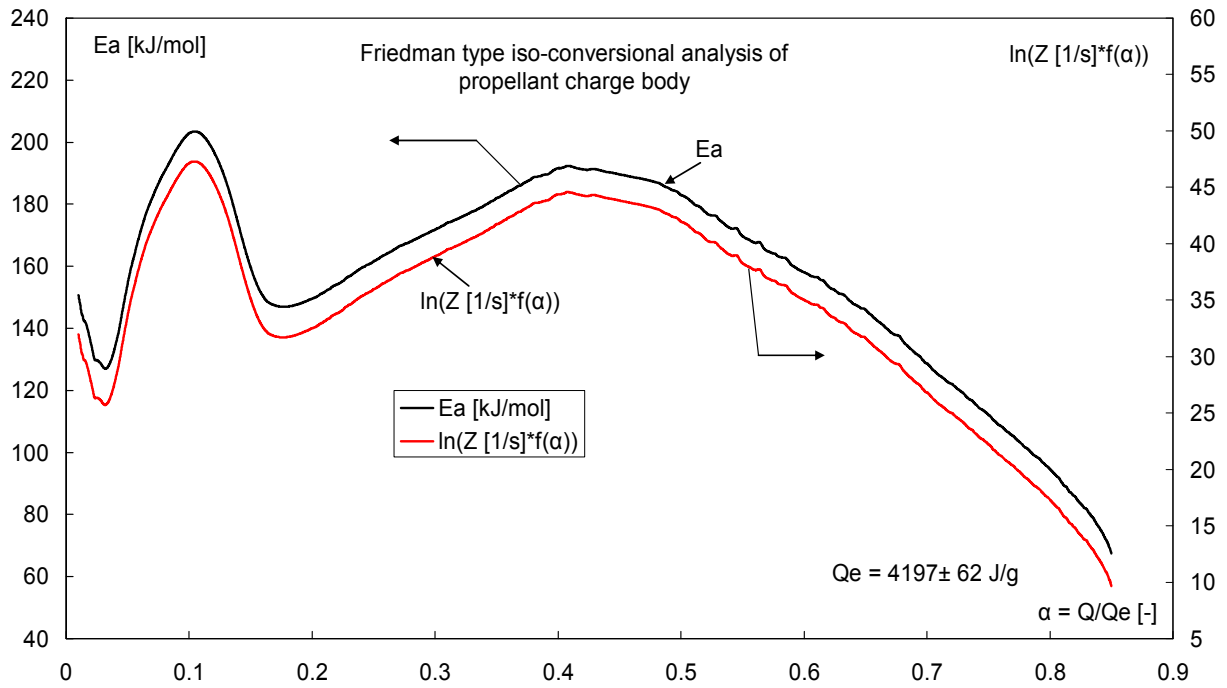


Fig. 20: Result of the Friedman analysis (=differential iso-conversional data analysis) of the DSC data of the propellant body. Activation energy and pre-exponential factor as function of conversion of the exothermal decomposition reaction.

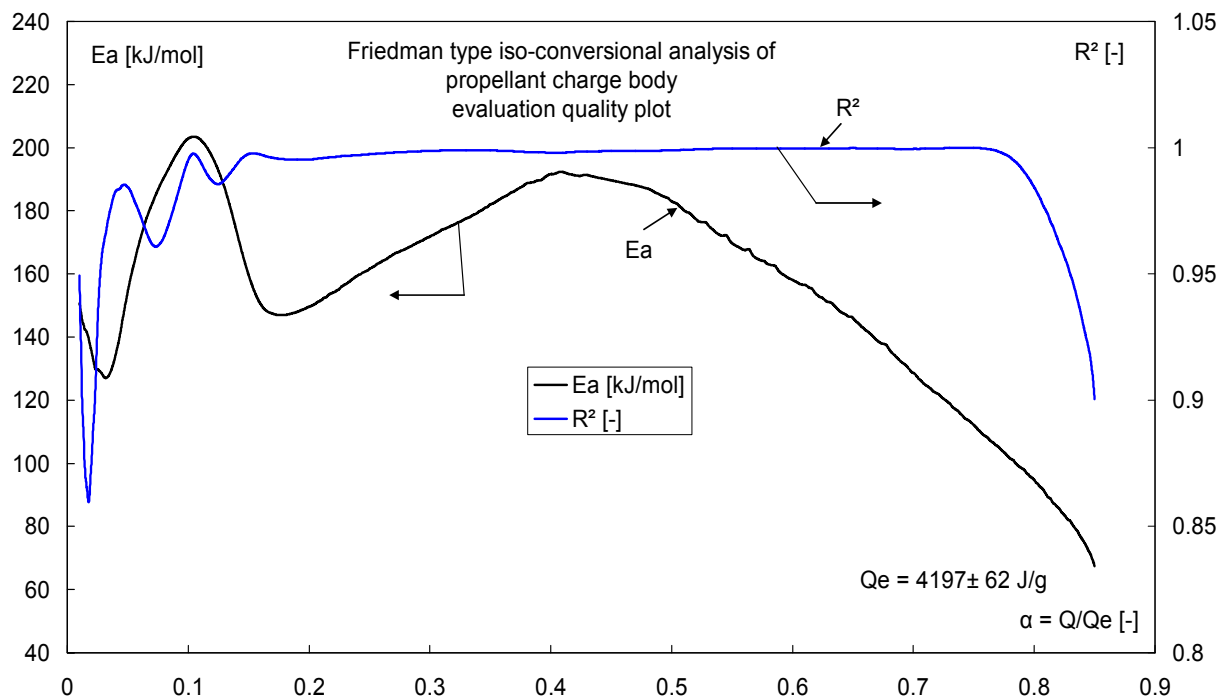


Fig. 21: Evaluation quality plot, showing the correlation coefficient of the Friedman analysis of the DSC data of the propellant body. Activation energy and correlation coefficient as function of conversion of the exothermal decomposition reaction.

3.3 Determination of heat conductivity and specific heat capacity of PB and PUR foam PU8

To perform the calculations the heat conductivity and the specific heat capacity of the materials involved must be known. For steel and air they are obtainable. The data for PB and PU8 must be measured. For this the so-named HotDisk™ instrument, model TPS 2500S, manufactured by Hot Disk AB, Gothenburg, Sweden, was used. Detailed description of this method can be found in /12, 13/. The thermal transport properties heat conductivity and thermal diffusivity are determined directly using the temperature increase of a transient plane heat source placed between two equal sample parts. The basic equation is given in Eq.(6), which relates heat conductivity λ , thermal diffusivity κ and volume specific heat capacity $c_{p,v}$.

$$(6) \quad \lambda = \kappa \cdot c_{p,v} \quad \text{or} \quad c_{p,v} = \lambda / \kappa$$

$$(7) \quad c_p = \frac{c_{p,v}}{\rho}$$

The mass specific heat capacity c_p is obtained from Eq.(7) by division of $c_{p,v}$ with the mass density ρ . For the evaluation the temperature increase ΔT of the sensor spiral, see /12,13/ with respect to the start temperature is used, which is described by Eq.(8).

$$(8) \quad \Delta T = A + \frac{P_0}{\pi^{3/2} \cdot a_s \cdot \lambda} \cdot D(\tau_c)$$

$$(9) \quad \tau = \sqrt{\frac{t}{\Theta}}$$

$$(10) \quad \Theta = \frac{a_s^2}{\kappa}$$

$$(11) \quad \tau_c = \sqrt{\frac{t - t_c}{\Theta}}$$

τ	dimensionless normalized time, not yet corrected for initial effects
t	measurement time
t_c	correction time interval, initial time period of the measurement, which is taken out from the evaluation
τ_c	corrected dimensionless normalized time
Θ	characteristic time of the measurement situation
κ	thermal diffusivity of the bulk of the material
a_s	characteristic length of the probing sensor, here the radius a_s of the disk
λ	heat conductivity (thermal conductivity) of the bulk of the material
P_0	total heating power of heat pulse, applied during the measurement
$D(\tau_c)$	dimensionless function depending on normalized time τ (here with τ_c) and geometrical parameters of the plane source and the probed material. Wave propagation function for a transiently acting plane source, see /13/.

By fitting the experimental data to Eq.(8) the two fitting parameters λ and κ are obtained, see /13/. The method assumes infinite extension of the sample. But by the choice of sensor radius (plane heat source) and measurement time this situation is simulated as pseudo infinite extension of the material. For this a certain size of the samples is necessary, in order to get an undisturbed propagation of the plane heat wave through the material. Moreover, if the material has any grain structure then the sensor radius, but at least the diameter, should about 10 times of the typical grain dimension. Here the sensor radius a_s was 9.87 mm.

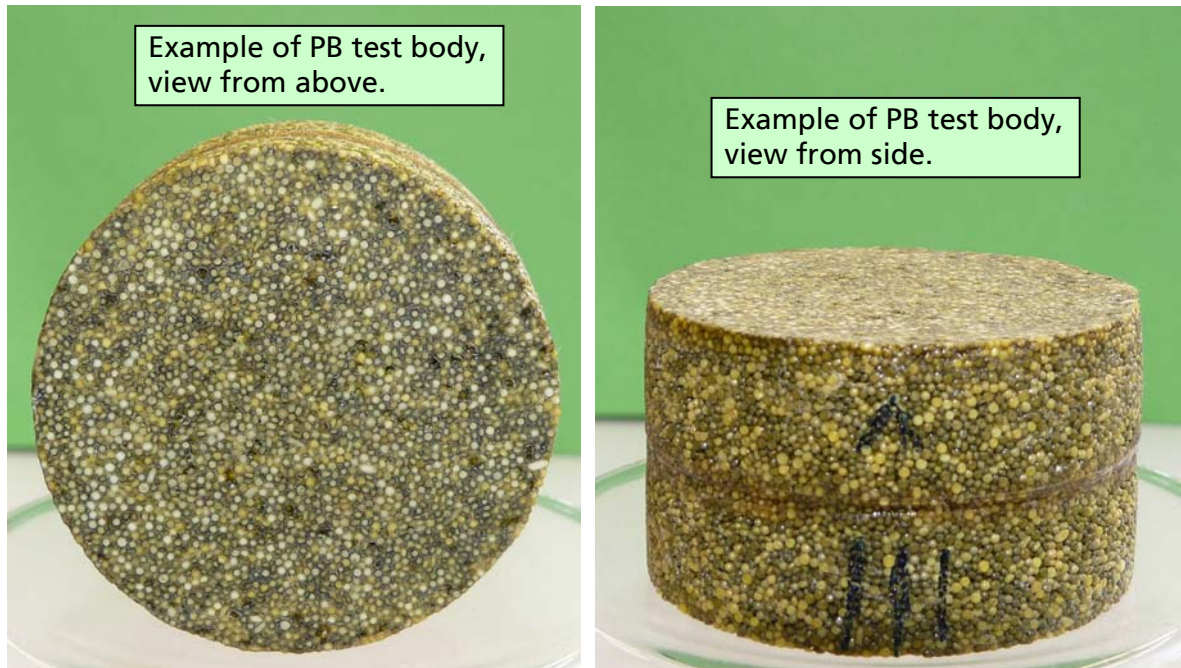


Fig. 22: Example of four PB samples especially manufactured for the determination of heat conductivity and specific heat capacity. PB samples made from ball powder with glued together balls with reduced graphite content. The diameter of these test samples is 48 mm and the height is about 28 mm. To reach the necessary height two disks have been glued together.

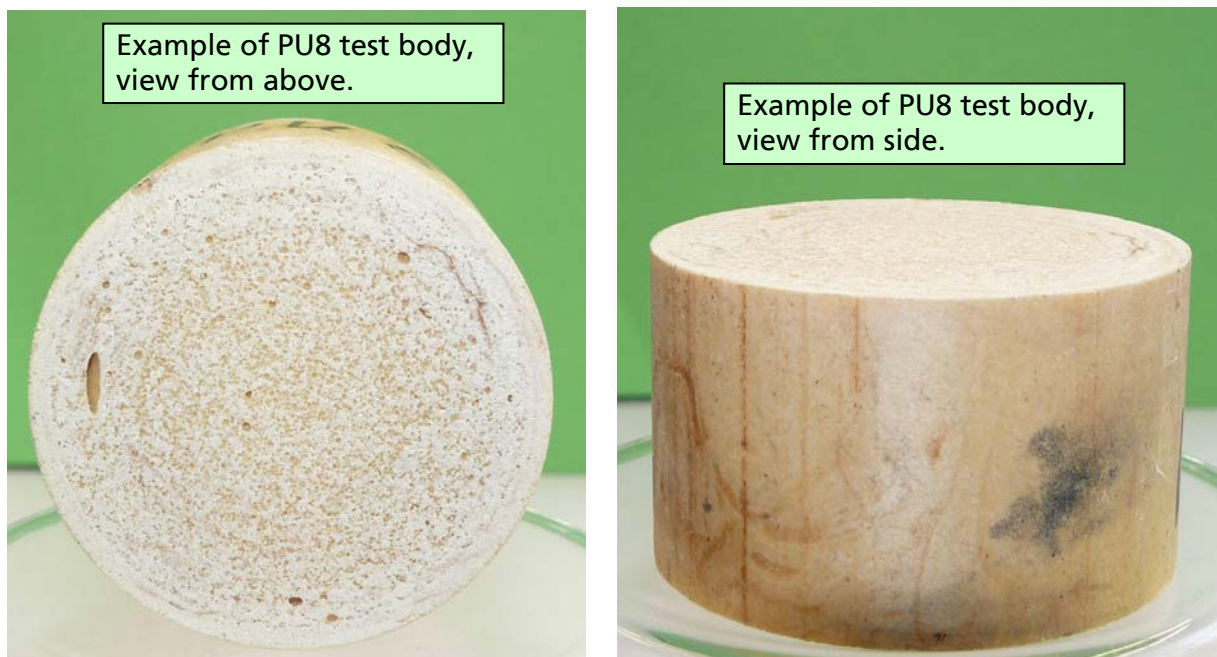


Fig. 23: Example of four PU8 samples especially manufactured for the determination of heat conductivity and specific heat capacity. They have been manufactured at Fraunhofer ICT. Their diameter is 50 mm, the height is 30 mm. The porous structure is well recognizable.

The Fig. 22 presents photographs of one of four PB test samples especially manufactured for the purpose of the determination of heat conductivity and specific heat capacity. One of four test sample of PU8 can be seen in Fig. 23. In Fig. 24 the transient graph is

shown, it is the temperature increase ΔT of the sensor (metal spiral) during the transient heating of the sample. The shape of the curve is influenced by the material. These data are used in the evaluation with Eq.(8). Table 6 lists all the properties needed for the calculations of the times to autoignition t_{Aig} at preset temperature T of the steel burning chamber. Additionally the activation energies and the pre-exponential factors as function of conversion given in section 3.2 are employed.

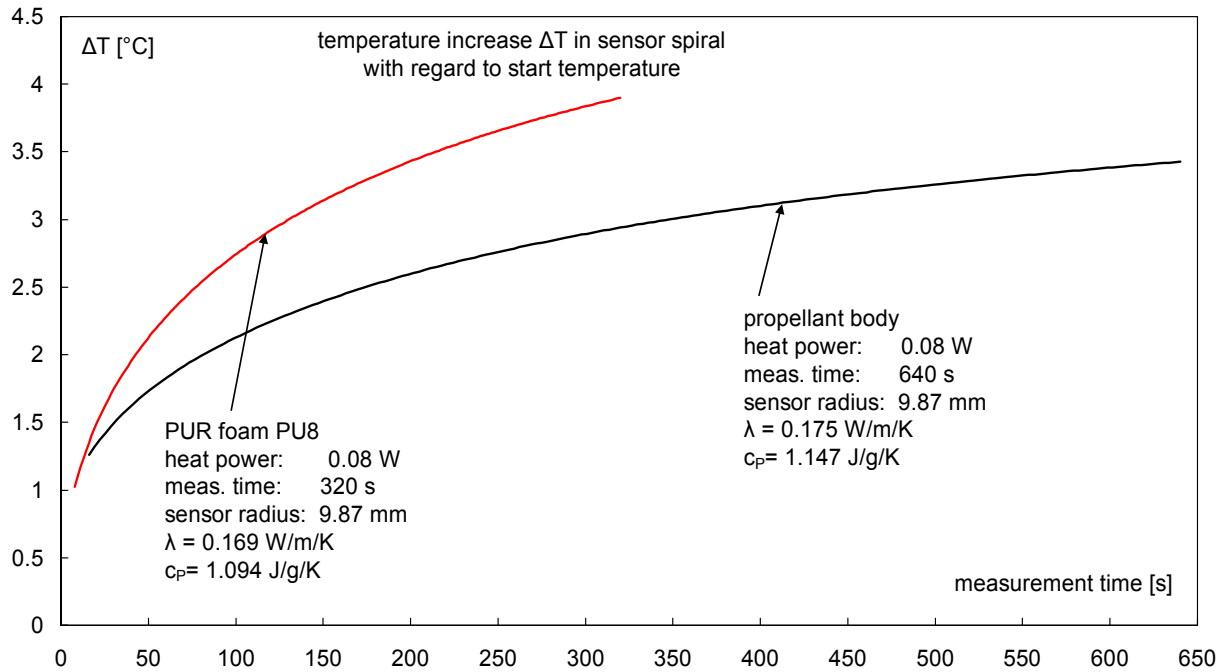


Fig. 24: So-named transient graph of the courses of the difference temperature ΔT with regard to the start temperature $T_A = 21^\circ\text{C}$ of the samples PB and PU8 as function of measurement time during the measurement with HotDisk™

Table 6: Compilation of the thermal properties of the materials involved in the FE simulation. Used heat transfer number h from the outside air to the steel: $h = 50$ W/cm²/K. The column $T_{Aig-Wood}$ gives the Autoignition temperatures determined in Wood metal bath at scanning temperature with 5°C/min and 0.2g sample amount.

material	λ [W/cm/K]	ρ [g/cm ³]	C_p J/g/K	$\kappa = \lambda/\rho/C_p$ [cm ² /s]	ΔQ_R [J/g]	$T_{Aig-Wood}$ at 5°C/min [°C]
PB	0.00175	1.53	1.147	0.000995	4197.38	171
PU8	0.0017	1.0	1.094	0.00155	1847.25	221
air	0.000251	0.00129	1.0	0.195	-	-
steel	0.396	7.85	0.46	0.11	-	-

λ	Heat conductivity, determined by HotDisk™ method
ρ	Mass density
C_p	Mass specific heat capacity, obtained via HotDisk™ determinations
κ	Thermal diffusivity, determined by HotDisk™ method
ΔQ_R	Decomposition reaction energy, determined via DSC in closed crucibles

3.3 FE calculations of the times to ignition t_{Aig} in the total charge

In the following the results of the calculation at 300°C are presented. Table 7 shows the set-up of the layers and their numbering: heat reservoir (0) – steel (1) – PU8 spacer (2) – PU8 coating on PB (3) – propellant body PB (4) - air in central bore of PB (5). Initial temperature of the steel is chosen, the other layers are always at 20°C at start condition. This set-up is always equal except for the initial temperatures in layers 0 and 1. In one calculation series the PU8 spacers and the PU8 coating have been taken as energetically inert, means no exothermal decomposition happens in these layers.

Table 7: Layer scheme of the simulation calculations with FE programme package, also called layer system 3, in which layer no. 2, 3 and 4 are energetic. A cylindrical geometrical arrangement was used.

Layer material	Layer thickness [mm]	Layer No.	Thermal decomposition in layer	Initial temp. [°C]	Heat transfer number h [W/cm ² /K]
Heat reservoir (air)		0	-	300	50
Steel	10	1	-	300	-
PU8 spacer	1.1	2	x	20	-
PU8 coating of PB	0.1	3	x	20	-
Propellant body (PB)	8.8	4	x	20	-
Central bore of PB	2.5	5	-	20	-

The Fig 25 shows the layer scheme in temperature-distance presentation, from the outside of the steel chamber to the center with the bore in the PB. The temperature course of the calculation with 300°C for the steel can be seen also. The temperature has already a little peak in the PU8 spacer indicating an ignition in the next tenth of a second, but the temperature in the PB charge has also reached or even surpassed the measured ignition temperature at 5°C/min heating rate, means that ignition will start also in the next few tenth of a second at the interface region of PB on the side of its PU8 coating. The next Figs 26 to 30 show the temperature courses in the five layers. The schemes always show the temperature distribution as function of time from the outside to the inside of the layer with 10 curves equally distributed over the thickness of the layer. In layer 1 (steel) one has also on the outside a cooling down because of heating up the charge, which was initially at 20°C. After about 28 seconds the charge starts to decompose significantly and heats up the steel. In layer 2, the PU8 spacer, a continuously heating up from initially 20°C can be seen. After about 28 seconds the charge starts to decompose significantly and heats up the steel, see upper part on the interface of PU8 spacer to the steel. Also in layer 3, PU8 coating on PB, one has continuously heating up from initially 20°C. After about 31 seconds the charge starts to decompose significantly, probably of sustained heating up from the decomposition heat of the PB. The temperature distribution in the coating is quite uniform over the thickness of this layer. In the PB charge, layer 4, one has again a steadily heating up from initially 20°C. After about 31 seconds the PB charge starts to decompose significantly on the side to the PU8 coating. The temperature distribution in the PB shows a distinct distribution over its thickness. On the side of the bore not any heating-up has started in the PB. In layer 5, the air in the bore of the propellant body PB, no heating-up is shown.

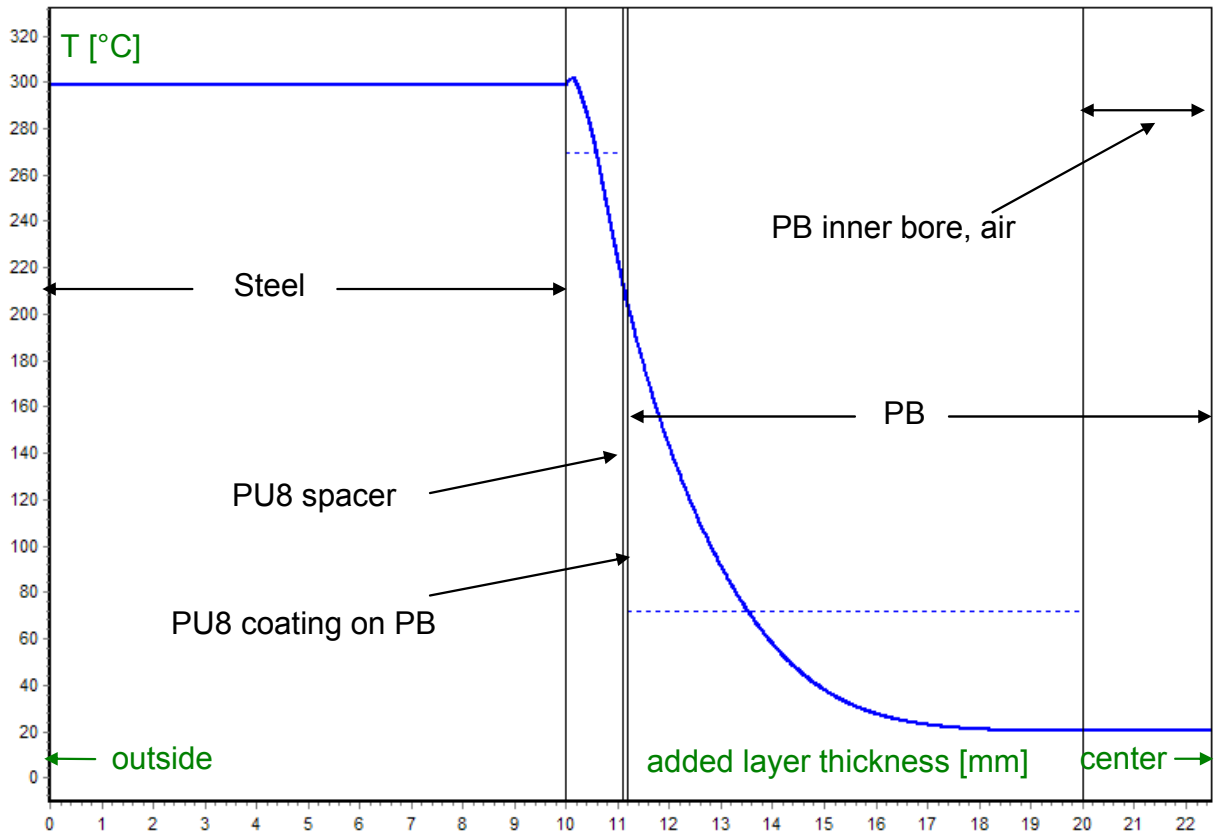


Fig. 25: Graphical presentation of the layer system used. Layer thicknesses are given in Table 7. The diagramme shows a calculation at 300°C. To be noted is the starting peak of the temperature in layer 2, the PU8 spacer.

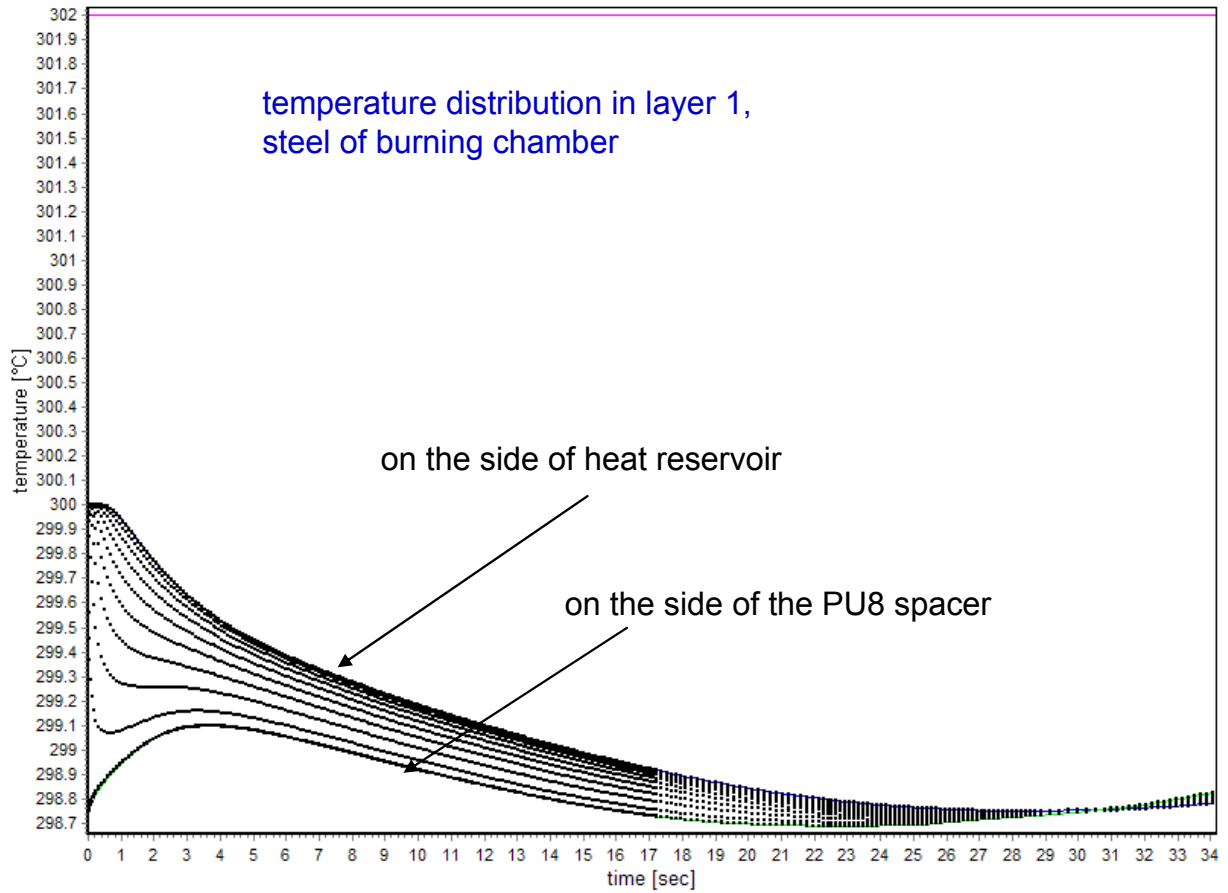


Fig. 26:

Calculation at 300°C. Temperature distribution as function of time in layer 1, the steel of the burning chamber. At first a cooling down in steel happens because of heating up the charge, which was initially at 20°C. After about 28 seconds the charge starts to decompose significantly and heats up the steel.

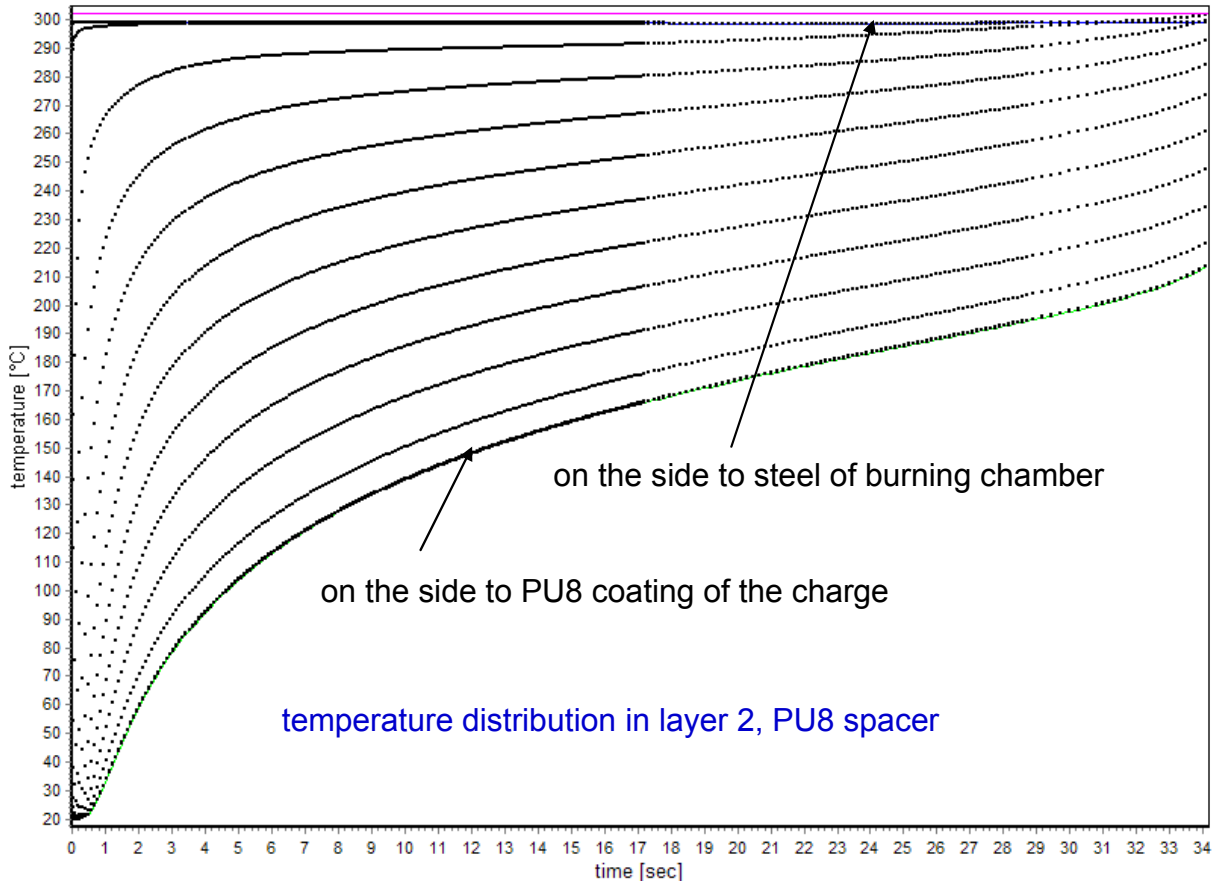


Fig. 27: Calculation at 300°C. Temperature distribution as function of time in layer 2, the PU8 spacer. Continuously heating up from initially 20°C. After about 28 seconds the charge starts to decompose significantly and heats up the steel, see upper part on the interface of PU8 spacer to the steel.

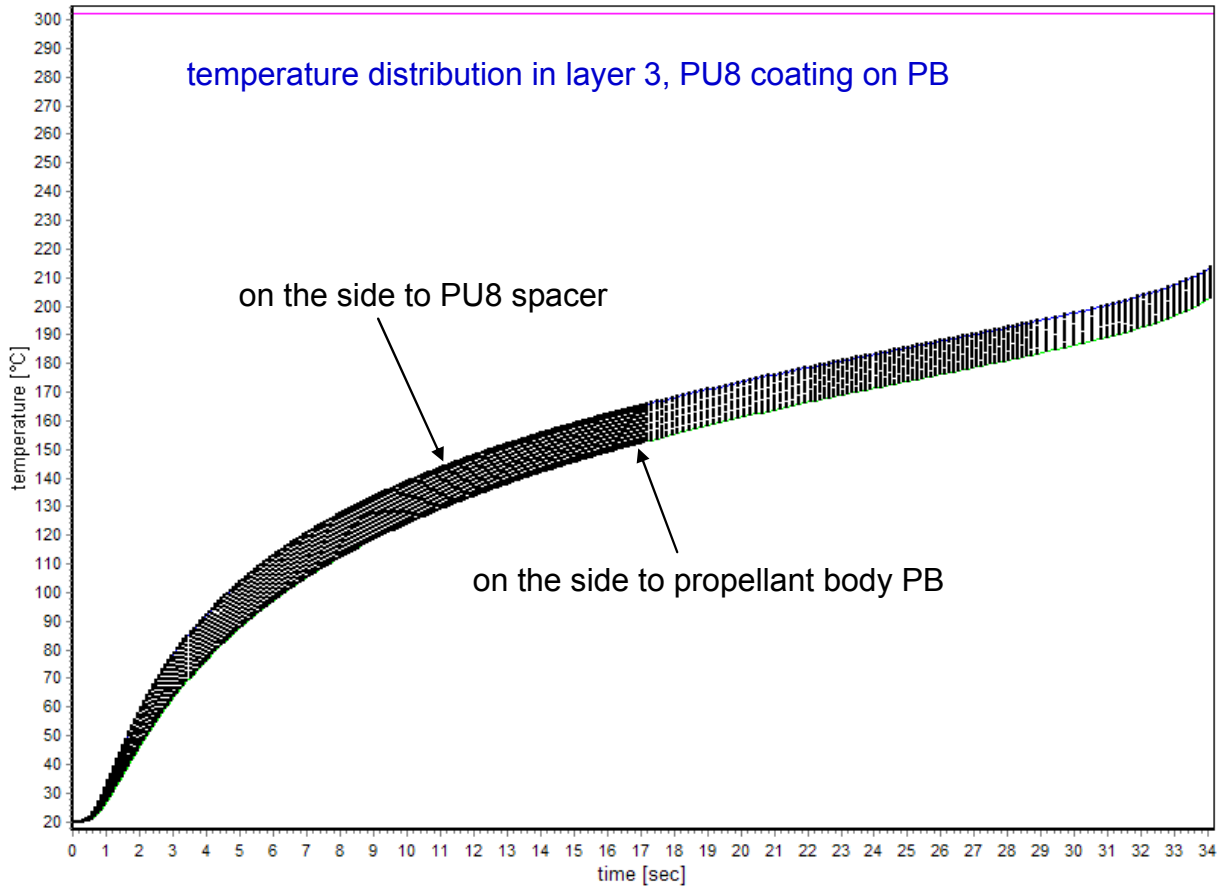


Fig. 28: Calculation at 300°C. Temperature distribution as function of time in layer 3, the PU8 coating on the propellant body PB. Steadily heating up from initially 20°C. After about 31 seconds the charge starts to decompose significantly, probably of sustained heating up from the decomposition heat of the PB. The temperature distribution in the coating is quite uniform over the thickness of this layer.

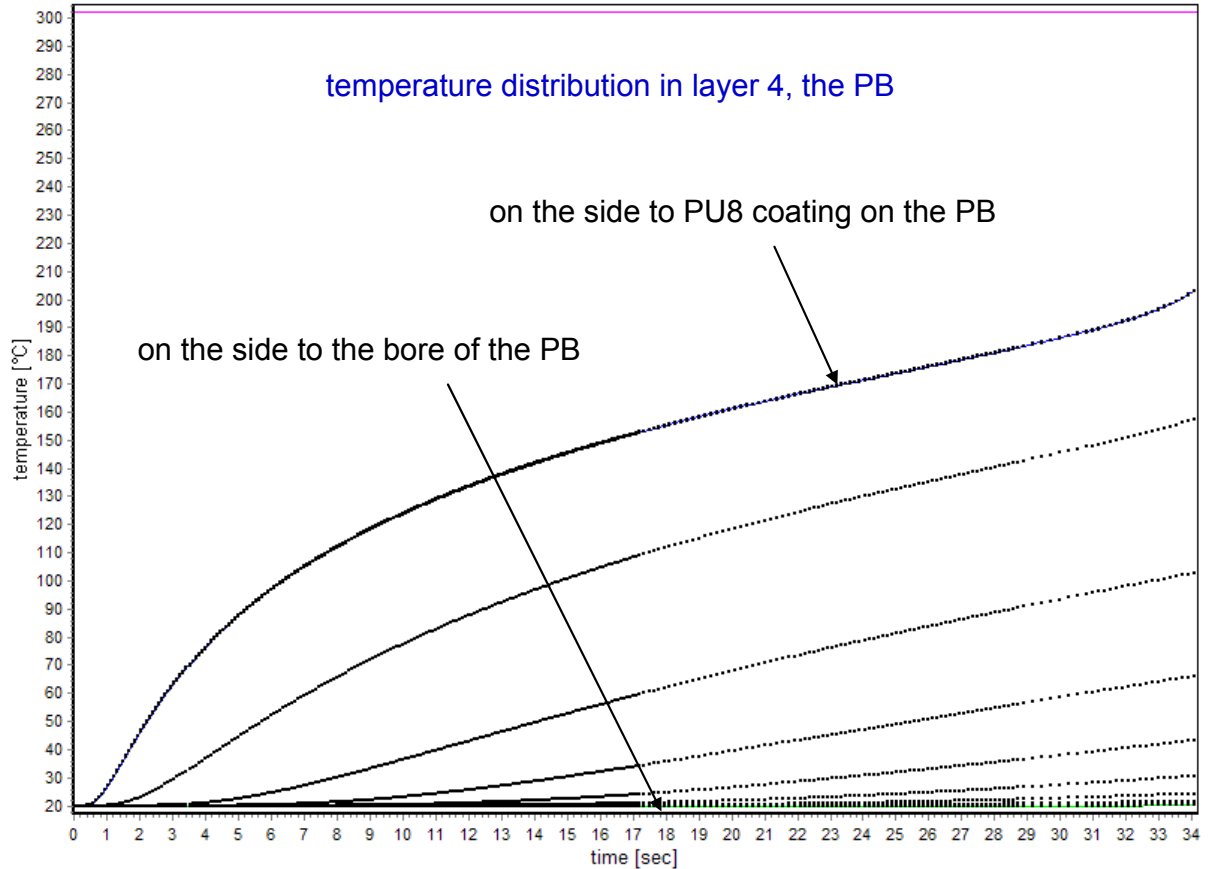


Fig. 29: Calculation at 300°C. Temperature distribution as function of time in layer 4, the propellant body PB. Continuously heating up from initially 20°C. After about 31 seconds the charge starts to decompose significantly on the side to the PU8 coating. The temperature distribution in the PB shows a distinct distribution over its thickness. On the side of the central bore in the PB the decomposition has not yet started.

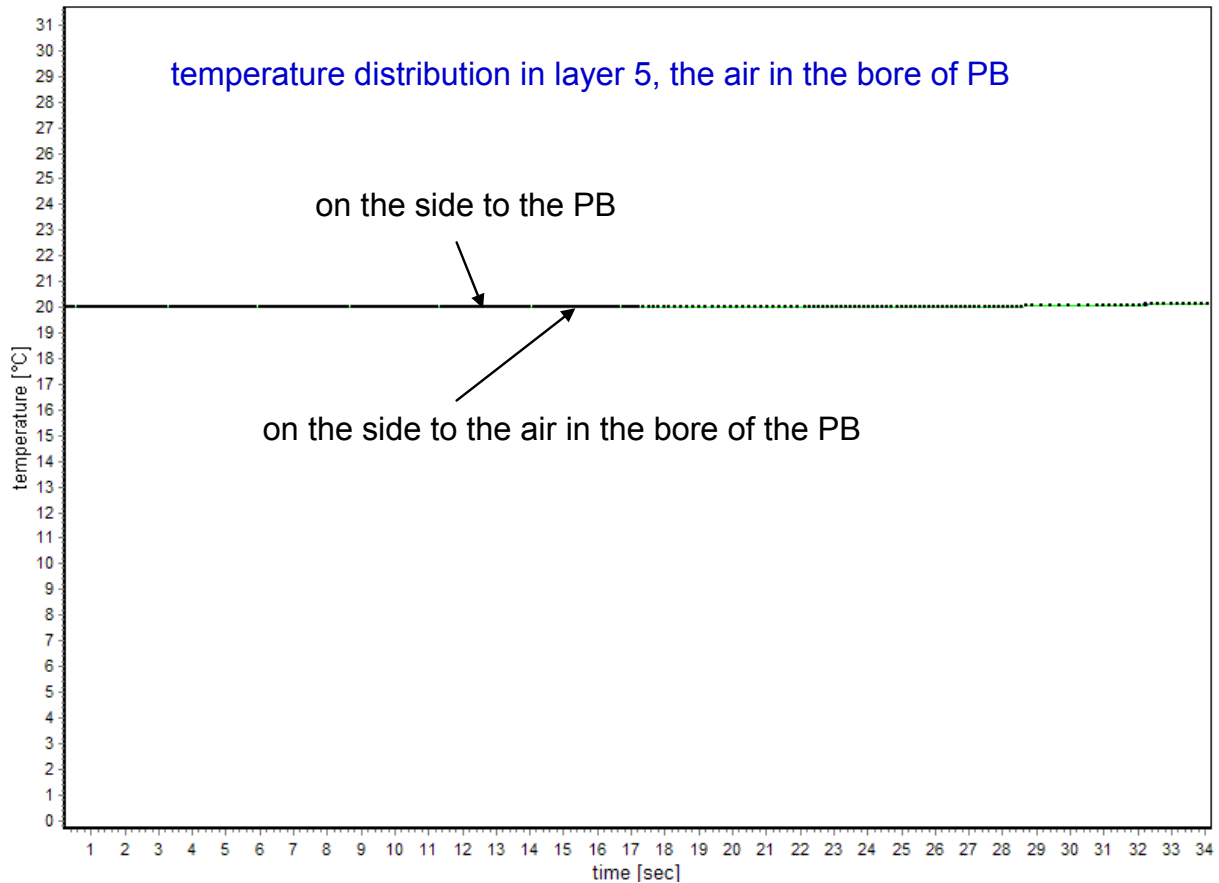


Fig. 30: Calculation at 300°C. Temperature distribution as function of time in layer 5, the air in the bore of the propellant body PB. No heating up in this layer at this preset temperature of 300°C.

In Table 8 the times to autoignition are listed as function of the load temperature, means the temperature of the steel burning chamber. The total propellant charge was always at 20°C. Two types of criteria have been applied. For PU8 and the PB a mean temperature T_m was taken (210°C and 190°C) and the times to reach these temperatures have been recorded as time to autoignition. The other criterion uses the time until the appearance of a little peak in the temperature course as shown in Fig. 25. This peak can arise in the PB or the PU8, depending on the load temperature. With the two criteria a time span arises for the time to autoignition in the temperature range 250°C to 360°C. This can be seen clearly in Fig. 31 and also in Fig. 32, which uses the absolute reciprocal temperature. From 250°C to lower temperatures ignition starts in the PB. From 350/360°C to higher temperatures ignition starts in PU8 spacer. In between these limits the ignition can start in PU8 or in the PB.

In part the time-temperature data follow Arrhenius plots, which are shown in Fig. 33 and Fig. 34. The corresponding apparent activation energies can be obtained. The activation energy for the ignition in the PB is with 41.4 kJ/mol quite low. Similar low values have been found by Turcotte a.o. with isothermal ARC measurements on NC in the temperature range 90 to 110°C. There the times to autocatalysis have been determined with activation energy of 76.6 kJ/mol /14/.

Table 8: Calculated times to autoignition as function of temperature of the steel burning chamber. Two types of criteria have been applied. For PU8 and the PB a mean temperature T_m was taken and the times to reach these temperatures have been recorded as time to autoignition. The other criterion uses the time until the appearance of a little peak in the temperature course as shown in Fig. 25.

T [°C]	time to reach $T_m=210^\circ\text{C}$ in PU8 [s]	time to reach $T_m=190^\circ\text{C}$ in PB [s]	time to ignition [s] seen as time to peak appearance in temperature
130			17985
130			12222
135			5052
140			2451
140			2079
150			1164
150			1114
160			762
160			672
160			764
170			544
180			378
190			292
190			306
200		223	228
200		229	234
210		177	183
220		140	146
230		112	120.3
240		91	99.6
250		74.5	83.4
250	43	75	83
255	32.5	69	76.8
260	27.4	63.7	70.9
270	15.7	52.5	60.7
280	12.6	46	51.5
290	8.39	36.7	43.9
300	6.61	31.4	32.5
310	4.75		21
310	4.75		21
320	3.9		13.2
330	2.99		8.7
340	2.6		5.7
345	2.32		3.7
350	2.07		2.75
360	1.77		1.91
370	1.39		1.41
380	1.08		1.08
390	0.852		0.852
400	0.675		0.675

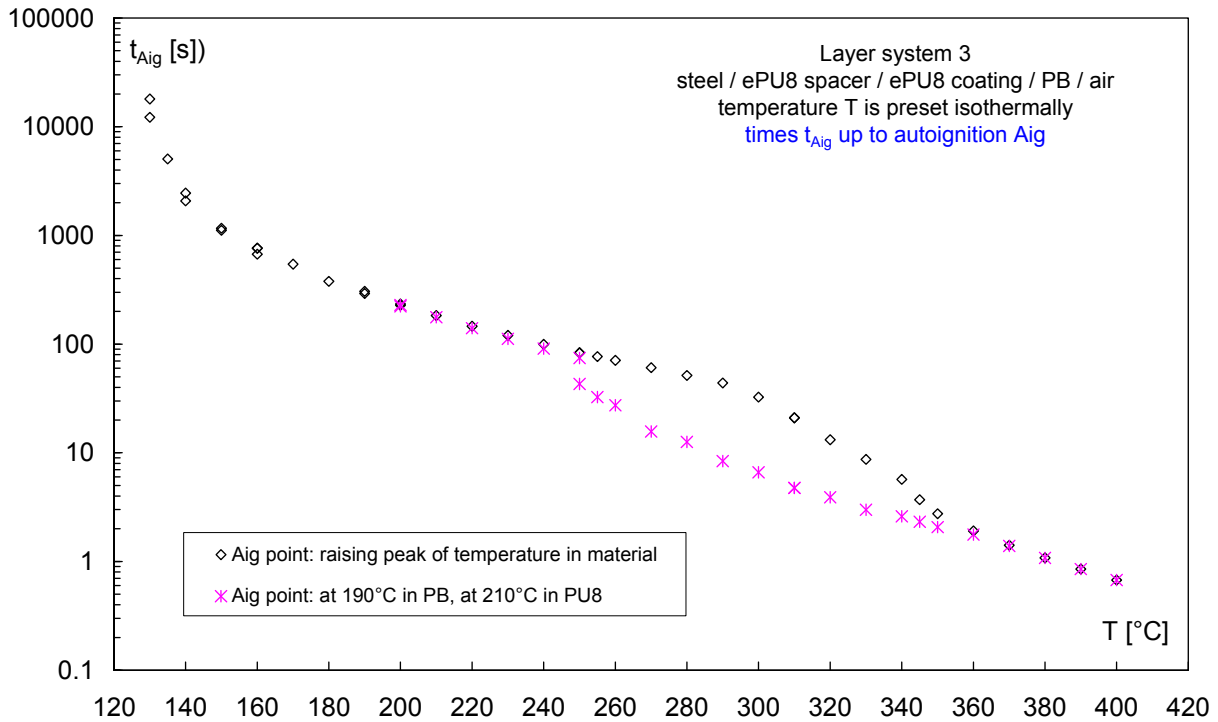


Fig. 31: Results of the FE calculations: time to autoignition t_{Aig} as function of temperature. Two criteria have been used to identify autoignition, which results in self-sustained burning: (i) The raising peak of the temperature in the material, as it is shown in Fig. 25 for layer 2, PU8 spacer; (ii) the reached temperature in the material, namely 190°C in PB and 210°C (average over layer) in PU8. In the temperature range 250°C to 350°C this results in an upper and a lower ignition curve.

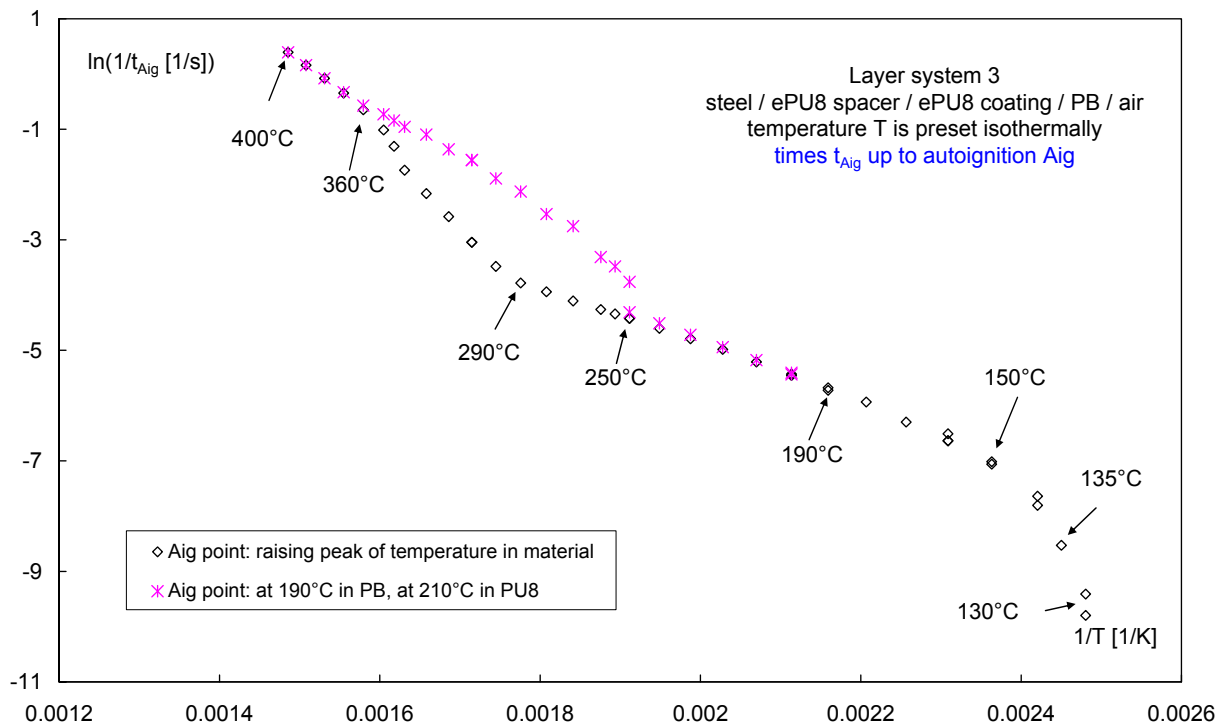


Fig. 32: Results of the FE calculations: time to autoignition t_{Aig} as function of reciprocal absolute temperature.

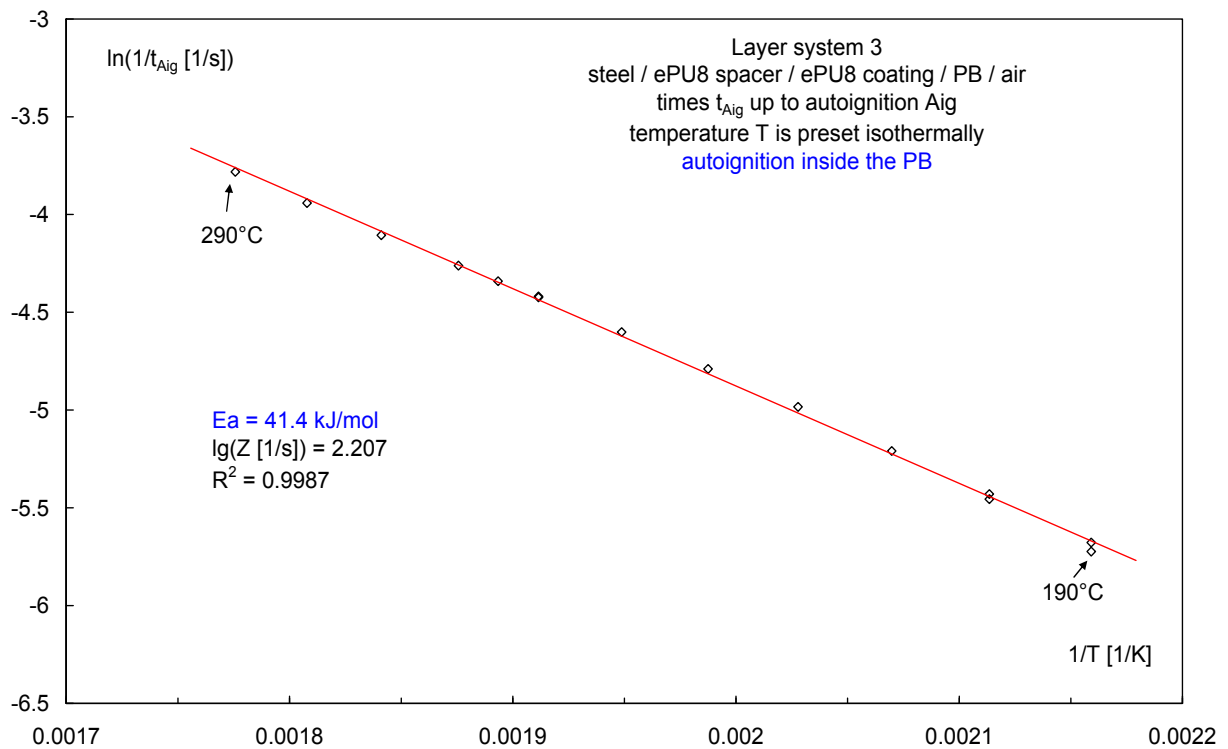


Fig. 33: Arrhenius plot of times to autoignition t_{Aig} in the lower temperature range, where the ignition starts in the NC-based PB. The activation energy is remarkably low.

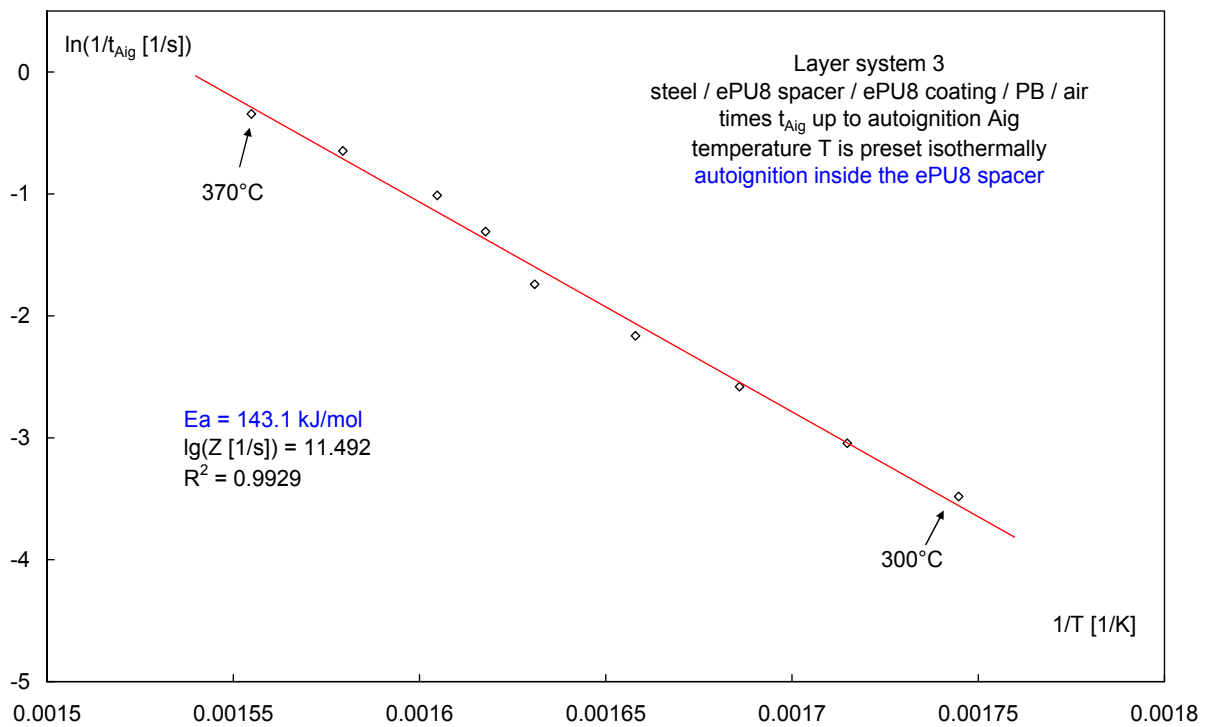


Fig. 34: Arrhenius plot of times to autoignition t_{Aig} in the upper temperature range, where the ignition starts in the PU8 foam.

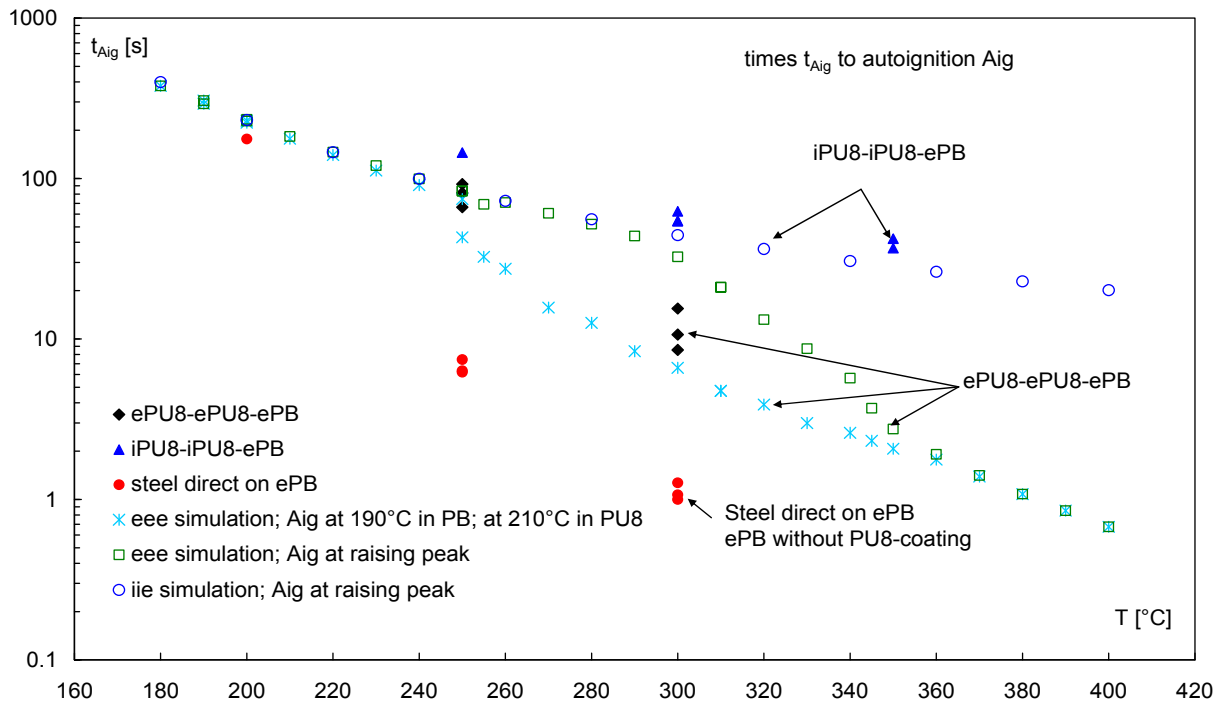


Fig. 35: Times to autoignition t_{Aig} as function of temperature. Calculations for two cases: (i) all three layers 2, 3, 4, are energetic; (ii) only the layer 4, the PB, is energetic, the PU8 layers are inert with respect to decomposition and heat production. Further to see are several real measurements made by company Diehl. The agreements between measurements and calculations are very good.

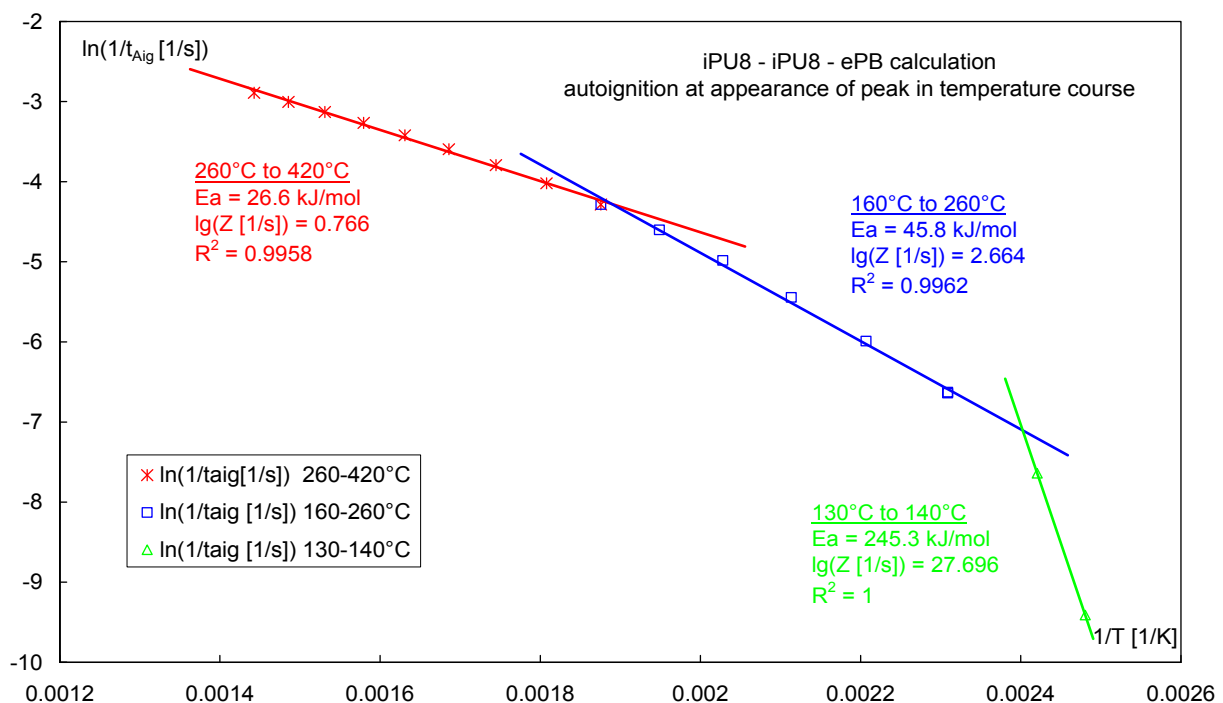


Fig. 36: Arrhenius plots of the times to autoignition t_{Aig} with the system inert PU8 spacer – inert PU8 coating – energetic PB. At high temperatures the activation energy is small indicating only a weak temperature dependence of t_{Aig} . At low temperatures the activation energy becomes great, indicating long times t_{Aig} and strong temperature dependence.

The Fig. 35 presents the comparison of calculated times to autoignition with the measured ones at 200°C, 250°C and 300°C, all three layers of the total charge are energetic. The agreement at 200°C and 250°C is very good. The measured data at 300°C show a scattering greater than at 250°C and 200°C. This reflects experimentally the 'ambiguous' or 'intermediate' situation found with the calculations. It means that the sustained burning may start from the PU8 spacer or from the propellant charge.

A further measurement and calculation series is presented in Fig. 36, namely the data obtained with inert PU8 as spacer and coating material and with energetic PB. Also in this case the agreement is very good. The Arrhenius plots of the times to autoignition t_{Aig} are presented in Fig. 33. The three quite different apparent activation energies represent the difference in temperature dependence of t_{Aig} .

4. Summary and conclusions

In the course of the development of a new high precision machine gun with caliber 12.7 mm a new concept of loading the bullet and the propellant charge was introduced by company Diehl. The charge is made from NC-NG based ball powder grains glued together. Because this charge was designed to be caseless, special measures have to be taken in order to prevent ignition of the charge by the hot burning chamber steel. This was achieved by spacers made from energetic foam based on PUR binder filled with 50 mass-% HMX. This material was developed at Fraunhofer ICT. Besides others two special tasks came out: (i) to achieve compatibility between the NC-NG-based propellant charge and the PUR foam; (ii) to prevent autoignition of the total charge by the heated up burning chamber steel after some firing.

At Fraunhofer ICT the compatibility tests were conducted on the base of heat flow microcalorimetric (HFMC) measurements. For this a special assessment procedure was applied already described earlier. This procedure is based on the allowed additional conversion. To get conversion with HFMC data, the appropriate reference values Q_{ref} have to be determined for each material combination under investigation. The way to get these data was shown. Finally one type of PUR foam was found and introduced as spacer and coating material for the PB charge.

To ensure that the weapon system has a good safety margin against autoignition of the propellant charge, Fraunhofer ICT performed FE calculations to determine the times to autoignition t_{Aig} under various conditions and a series of temperatures of the burning chamber steel in the range of 130°C to 420°C. The calculations provided with times much longer than the cycle time of the weapon. This means the automatic deloading after each loading and firing removes charges, which have been eventually not ignited during the firing cycle, much faster than the shortest reasonably assumable time to autoignition. The calculations have been verified by measurements made by company Diehl. The agreement between calculations and measurements is very good.

5. Abbreviations

BP	Ball powder, double base (with about 10 mass-% nitroglycerine, AkII stabilized), the here used lot version has low graphite content
PB	Propellant body, consolidated charge, ball powder grains glued together
A5023	20 mm gun propellant, single base, DPA stabilized
NC	nitrocellulose
NG	nitroglycerine
AK II	Acardite II, stabilizer for NC-based propellants
DPA	Diphenylamine, stabilizer for single base propellants
PUR	polyurethane
PU8	PUR foam type, 50 mass-% HMX, inert PUR-binder
PU9	PUR foam type, 50 mass-% HMX, energetic PUR-binder based on GAP
FE	Finite element calculation
t_{Aig}	Time to autoignition
HFMC	Heat flow microcalorimeter
DSC	Differential scanning calorimeter
HGR	Heat generation rate, dQ/dt , determined with microcalorimeter
HG	Heat generation, Q , determined from HGR by integration over time
dQ/dt	same as HGR
Q	same as HG
dR_Q/dt	Reactivity rate function, determined with heat generation rates
R_Q	Reactivity function, determined from HGs or by integration of dR_Q/dt
λ	Heat conductivity, determined by HotDisk™ method
c_p	Mass specific heat capacity, obtained via HotDisk™ determinations
κ	Thermal diffusivity, determined by HotDisk™ method
$c_{p,v}$	Volume specific heat capacity, $c_{p,v} = \lambda/\kappa$
ρ	Mass density
ΔQ_R	Decomposition reaction energy or reaction heat, determined via DSC in closed crucibles, in energy per mass
ΔH_R	Decomposition reaction enthalpy, in energy per mass, determined via DSC by $\Delta H_R = \Delta Q_R + \Delta n_R(\text{decomposition gases}) \cdot RT$; Δn_R is the change in mol numbers per mass of educt of the gases during the reaction, which are assumed to behave as perfect gases.

6. References

- /1/ A. Pfersmann, R. Himmert, A. Eckel.
System Munition ohne Hülse (MoH)
 Presentation on Wehrtechnisches Symposium 'Ballistik in Forschung und Technologie 2011' 19. bis 21. September 2011, BAKWVT, Mannheim, Germany.
- /2/ Jutta Böhnlein-Mauss, Angelika Eberhardt.
Foamed Propellants
 Propellants, Explosives, Pyrotechnics 27 (2002) 156 - 160.

- /3/ J. Böhnlein-Mauss, B. Scheidt, A. König, A. Pfatteicher, H. Popp, H. Kröber.
Foamed Propellants
P172 in Proceedings of 36th International Annual Conference of ICT 2005 on 'Energetic Materials', Karlsruhe, Germany. ISSN 0722-4087. Fraunhofer-Institut fuer Chemische Technologie (ICT), D-76318 Pfinztal. Germany.
- /4/ Manfred A. Bohn.
Generic formulation of performance assessment quantities for stability, compatibility and ageing of energetic materials.
Paper 59, pages 59-1 to 59-34 in Proceedings of the 43rd International Annual Conference of ICT on 'Energetic Materials – Synthesis, Characterisation, Processing', June 26 to 29, 2012, Karlsruhe, Germany. ISSN 0722-4087. Fraunhofer-Institut fuer Chemische Technologie (ICT), D-76318 Pfinztal. Germany.
- /5/ NATO STANAG 4147, edition 3, 2008.
Chemical Compatibility of Ammunition Components with Explosives (Non-Nuclear Applications).
Military Agency for Standardization, NATO Headquarters, Brussels, Belgium.
- /6/ NATO Standardization Agreement (NATO STANAG) 4582 '*Explosives, Nitrocellulose Based Propellants, Stability Test Procedure and Requirements Using Heat Flow Calorimetry*'
Military Agency for Standardization, NATO Headquarters, Brussels, Belgium.
- /7/ NATO Allied Ordnance Publication (NATO AOP) 48, edition 2
Explosives, Nitrocellulose-based Propellants, Stability Test Procedures and Requirements Using Stabilizer Depletion.
Military Agency for Standardisation, NATO Headquarters, 1110 Brussels, Belgium.
- /8/ Manfred A. Bohn.
Safety analysis of a single base propellant for automotive use with heat generation rate.
Paper 116, pages 116-1 to 116-26, in Proceed. of 41th International Annual Conference of ICT on 'Energetic Materials – High Performance, Insensitive Munitions, Zero Pollution', June 29 to July 2, 2010, Karlsruhe, Germany. ISSN 0722-4087. Fraunhofer-Institut für Chemische Technologie (ICT), D-76318 Pfinztal-Berghausen.
- /9/ Henry L. Friedman.
Kinetics of thermal degradation of char-forming plastics from thermogravimetry. Application to a phenolic plastic.
J. Polymer Science Part C: Polymer Symposia, Volume 6, Issue 1 (1964) 183-195.
<http://www3.interscience.wiley.com/journal/114174147/issue>
- /10/ AKTS Advanced Thermokinetics Software.
AKTS AG - Advanced Kinetics and Technology Solutions,
TECHNOArk 3, 3960 Siders, Switzerland. <http://www.akts.com>
- /11/ Bertrand Roduit.
Computational aspects of kinetic analysis. Part E: The ICTAC Kinetics Project - numerical techniques and kinetics of solid state processes.
Thermochimica Acta 355 (2000) 171-180.

- /12/ Manfred A. Bohn, Kerstin Hartlieb, Heike Pontius.
Thermal transport properties of energetic materials determined by a transient probing method.
Paper 79, pages 79-1 to 79-10, in Proceed. of 41th International Annual Conference of ICT, June 29 to July 2, 2010, Karlsruhe, Germany. ISSN 0722-4087. Fraunhofer-Institut für Chemische Technologie (ICT), D-76318 Pfinzthal-Berghausen
- /13/ Heike Pontius, Manfred Bohn.
Determination of the thermal properties heat conductivity, thermal diffusivity and specific heat by the HotDisk™ instrument.
Paper 58, pages 58-1 to 58-14 in Proceedings of the 43rd International Annual Conference of ICT on 'Energetic Materials – Synthesis, Characterisation, Processing', June 26 to 29, 2012, Karlsruhe, Germany. ISSN 0722-4087. Fraunhofer-Institut fuer Chemische Technologie (ICT), D-76318 Pfinzthal. Germany.
- /14/ R. Turcotte, B. Acheson, S. Singh and M. Paquet
Effect of Pressure on the Thermal Decomposition of Nitrocellulose and its Mixtures with Nitroglycerin.
CANMET Canadian Explosives Research Laboratory. Report (2006)